Journal of the Mechanics and Physics of Solids 78 (2015) 70–93

Contents lists available at ScienceDirect

Journal of the Mechanics and Physics of Solids

journal homepage: www.elsevier.com/locate/jmps

Steady and transient sliding under rate-and-state friction

Thibaut Putelat [a,b,*], Jonathan H.P. Dawes [c]

[a] Department of Engineering Mathematics, University of Bristol, Faculty of Engineering, Queen's Building, University Walk, Bristol BS8 1TR, UK
[b] Laboratoire de Mécanique des Solides, UMR–CNRS 7649, École Polytechnique, 91128 Palaiseau, France
[c] Department of Mathematical Sciences, University of Bath, Claverton Down, Bath BA2 7AY, UK

ARTICLE INFO

Article history:
Received 14 March 2014
Received in revised form
7 January 2015
Accepted 31 January 2015
Available online 3 February 2015

Keywords:
Stiction loss
Stick-slip
Friction angle
Bistability
Non-monotonic friction
Slope stability
Landslide

ABSTRACT

The physics of dry friction is often modelled by assuming that static and kinetic frictional forces can be represented by a pair of coefficients usually referred to as μ_s and μ_k, respectively. In this paper we re-examine this discontinuous dichotomy and relate it quantitatively to the more general, and smooth, framework of rate-and-state friction. This is important because it enables us to link the ideas behind the widely used static and dynamic coefficients to the more complex concepts that lie behind the rate-and-state framework. Further, we introduce a generic framework for rate-and-state friction that unifies different approaches found in the literature.

We consider specific dynamical models for the motion of a rigid block sliding on an inclined surface. In the Coulomb model with constant dynamic friction coefficient, sliding at constant velocity is not possible. In the rate-and-state formalism steady sliding states exist, and analysing their existence and stability enables us to show that the static friction coefficient μ_s should be interpreted as the local maximum at very small slip rates of the steady state rate-and-state friction law.

Next, we revisit the often-cited experiments of Rabinowicz (*J. Appl. Phys.*, 22:1373–1379, 1951). Rabinowicz further developed the idea of static and kinetic friction by proposing that the friction coefficient maintains its higher and static value μ_s over a *persistence length* before dropping to the value μ_k. We show that there is a natural identification of the persistence length with the distance that the block slips as measured along the stable manifold of the saddle point equilibrium in the phase space of the rate-and-state dynamics. This enables us explicitly to define μ_s in terms of the rate-and-state variables and hence link Rabinowicz's ideas to rate-and-state friction laws.

This stable manifold naturally separates two basins of attraction in the phase space: initial conditions in the first one lead to the block eventually stopping, while in the second basin of attraction the sliding motion continues indefinitely. We show that a second definition of μ_s is possible, compatible with the first one, as the weighted average of the rate-and-state friction coefficient over the time the block is in motion.

* Corresponding author at: Department of Engineering Mathematics, University of Bristol, Faculty of Engineering, Queen's Building, University Walk, Bristol BS8 1TR, UK.
E-mail addresses: t.putelat@bristol.ac.uk (T. Putelat), J.H.P.Dawes@bath.ac.uk (J.H.P. Dawes).

http://dx.doi.org/10.1016/j.jmps.2015.01.016
0022-5096/

1. Introduction

It has long been recognised that the force required to initiate sliding between two solid interfaces in (dry) frictional contact is usually greater than the force needed to sustain sliding, see Persson (2000) for a brief historical summary. This behaviour of solid frictional contact led to the distinction between the static and dynamic coefficients of friction, denoted μ_s and μ_k respectively, and forms the basics of Coulomb's model of friction (Bowden and Tabor, 1954; Rabinowicz, 1995; Persson, 2000). Although being a convenient simplified description of the physics of friction, considering these two coefficients as different constants allows a first account to be made of the motion of a rigid block sliding on an inclined surface or the classical stick-slip phenomenon which characterises the saw-tooth dynamics of spring–block systems (Bowden and Tabor, 1954) and is also pertinent to many engineering situations as well as a source of stimulating mathematical problems, e.g. see Duvaut and Lions (1976) and di Bernardo et al. (2008) for examples with emphasis on piecewise-smooth dynamical systems models relevant to friction.

However, several decades and many studies have been required to shed light on the physical processes at the origin of the apparent non-smooth nature of the frictional force, either for dry or lubricated frictional interfaces (e.g. Rabinowicz, 1951; Berthoud et al., 1999; Baumberger et al., 1999; Persson et al., 2003). Noticeably, it was recognised early on that explaining the variation of the amplitude of stick-slip oscillations, as observed experimentally, requires consideration of the velocity-dependence of kinetic friction and the time-of-stick dependence of static friction together with the past history of sliding, see Rabinowicz (1957, 1995) and references therein. Indeed, Rabinowicz (1957) argued that the memory of sliding over some preceding critical distance also affects the value of the kinetic friction coefficient and determines the shape of the stick-slip cycle.

The framework of rate-and-state friction allows these three main physical ingredients to be unified into a single phenomenological theory of friction (Dieterich, 1979; Ruina, 1980, 1983; Rice and Ruina, 1983; Gu et al., 1984). In effect, the concept of rate-and-state friction makes possible the link between the two friction coefficients by recognising that the logarithmic time variation of μ_s and the velocity dependence of μ_k both result from the complex evolution of asperities in interfacial contact, controlled by some characteristic memory length (Dieterich, 1979). Roughly speaking, the true contact area increases from the creep of asperities in stationary contact while the contact population is rejuvenated during interfacial sliding (e.g. Heslot et al., 1994). This phenomenology can be captured by introducing internal variables which characterise the interfacial state and whose evolution is governed by empirical nonlinear evolution equations measuring the departure from or relaxation to an equilibrium interfacial state (Rice et al., 2001).

In the rate-and-state friction formalism it is not possible to make a clear distinction between static and dynamic friction coefficients. Nevertheless a static coefficient is often defined as the peak value of the friction coefficient which follows a sudden interfacial slip like the one promoted in slide-hold-slide experiments performed with a spring-block system (Dieterich, 1979; Beerler et al., 1994; Berthoud et al., 1999). The time dependence of this static friction coefficient corresponds to the holding time before sudden slippage or velocity variation.

We adopt in this paper a complementary viewpoint and work backwards towards the empirical distinction between static and dynamic friction coefficients by analysing the motion of a block which slides on an inclined slope. This is the simplest situation that allows the study of the transient frictional slip dynamics, starting from rest and subjected to a constant gravitational driving force. From consideration of the stability of such a sliding configuration, our first result is an interpretation of the static friction coefficient as the local maximum of the steady-state friction coefficient at very small slip rates.

Next, we revisit the impact experiment of Rabinowicz (1951) who studied the response of the block to the impulse provided by the elastic impact of a rolling ball. When friction is velocity-weakening, we can identify Rabinowicz's persistence length (over which, in Rabinowicz's proposal, the friction coefficient is taken to keep its static value), as the block slip distance as measured along the stable manifold which divides the phase space into sets of initial conditions that ultimately lead to either eventual rest or unbounded sliding. We compare the persistence length with the memory length associated with rejuvenation of the interfacial state; this analysis leads to a second definition of the static friction coefficient as the weighted average of the dynamic friction coefficient during motion.

Overall we advocate, on primarily mathematical grounds, the necessity of rate-and-state friction models whose steady-state velocity dependence is not monotonic, and in their most complicated form correspond to a 'spinodal' (i.e. *N*-shaped) dependence. Moreover, this theoretical need (so that the mathematical model is well-posed) is supported by many experimental observations obtained with various materials. These indicate the existence of crossovers between velocity-weakening and velocity-strengthening friction regimes, albeit attributed to diverse microphysical mechanisms. Examples include Grosch, 1963 for rubber, Shimamoto (1986), Weeks (1993), Kilgore et al. (1993), Tsutsumi and Shimamoto (1997) for rocks, and Heslot et al. (1994) for paper. A recent concise review is given by Bar-Sinai et al. (2014). We note also the physical considerations discussed and developed by Bréchet and Estrin (1994), Estrin and Brechet (1996) and Baumberger and Caroli (2006) and the examples of applications given in our previous work (Putelat et al., 2007, 2008, 2010).

The structure of the paper is as follows. In Section 2 we review the construction of rate-and-state friction laws. We propose a general framework from which several well-known specific constructions follow through different choices of various functional forms. We describe briefly how the regularised 'spinodal' law, that we have proposed in earlier work, also fits into this framework. In Section 3 we discuss the dynamics of a block sliding on a slope at a fixed angle, under different choices of rate-and-state friction law, concentrating on the spinodal case. Section 4 discusses the impact experiments

carried out by Rabinowicz, and uses the rate-and-state framework to re-interpret and understand his results. Section 5 concludes and discusses various consequences of our results, in particular within geophysical settings such as fault mechanics and the earthquake nucleation phase as well as the stability of slopes and landslides and their sensitivity to finite amplitude perturbations in relation to spinodal friction.

2. Rate-and-state friction

Rate-and-state friction laws are phenomenological models for sliding interfaces that, from one point of view, can be seen as a mechanism for introducing higher order corrections in order to regularise the traditional discontinuous Coulomb model of friction. Typically rate-and-state equations are constructed by assuming that the frictional stress depends, in addition to the usual normal stress parameter, on both the instantaneous slip velocity and on one or more state variables describing the sliding ability (loosely speaking referred to as the 'roughness'[1]) of the interface. These state variables effectively introduce a memory of the past evolution of the interfacial slip rate, allowing more complicated dynamical evolution of the system (Dieterich, 1978, 1979; Ruina, 1980, 1983; Rice and Ruina, 1983). The memory effects modelled by the state variables evolve through empirical evolution equations which attempt to capture the macroscopic behaviour resulting from complex interactions between microscale asperities on the interfaces.

Various different analytical expressions for rate-and-state models have been introduced over the years, especially regarding the interfacial state evolution law (see e.g. Ruina, 1983; Gu et al., 1984; Weeks, 1993; Heslot et al., 1994; Perrin et al., 1995; Rice and Ben-Zion, 1996; Baumberger and Caroli, 2006; Putelat et al., 2007, 2010). The literature in which experimental data is used to discriminate between these different models remains unfortunately sparse. We emphasised previously that the analytical details of the rate-and-state law matter in determining the nonlinear dynamics of friction, see Putelat et al. (2010). With this in mind, we present in this section a very brief overview of a general framework for rate-and-state models within which a number of commonly used models can be placed. This clarifies the relationship between them, and the relationship to the spinodal law that we introduced and discussed in a number of recent papers (Putelat et al., 2007, 2008, 2010, 2011). These different choices are summarised for convenience in Table 1.

Provided that thermal effects remain negligible, i.e. for sliding velocities well below the flash temperature critical velocity (Archard, 1959), rate-and-state constitutive laws are specified (Rice et al., 2001) by pairs of (dimensional) equations in the form

$$\tilde{\tau} = F(\tilde{v}, \tilde{\phi}; \tilde{\sigma}), \quad \text{and} \quad d\tilde{\phi}/dt = -G(\tilde{v}, \tilde{\phi}; \tilde{\sigma}), \tag{1}$$

where $\tilde{\tau}$ and $\tilde{\sigma}$ are the interfacial shear and normal stresses, respectively. The interfacial slip rate $\tilde{v}$ is defined by $\tilde{v} = \dot{\tilde{\delta}}$ where $\tilde{\delta} \equiv \tilde{u}_+ - \tilde{u}_-$ is the interfacial slip; this is the relative displacement in the direction of sliding. The state variable $\tilde{\phi}$ models the 'roughness' (slip resistance) of the interface; the time evolution $(1)_2$ describes the frictional memory effects. Throughout this section, dimensional variables are given tildes $\tilde{\cdot}$ in order to distinguish them from dimensionless variables.

Commonly used realisations of such laws (e.g. Scholz, 1998; Marone, 1998; Scholz, 2002) use the same formula for the friction coefficient $\mu(\tilde{v}, \tilde{\phi})$:

$$\mu \equiv \tilde{\tau}/\tilde{\sigma} = \mu_* + a \ln(\tilde{v}/V_*) + b \ln(\tilde{\phi}/\tilde{\phi}_*), \tag{2}$$

where μ_*, V_* and $\tilde{\phi}_*$ are reference values of the friction coefficient, velocity and the state variable, respectively, and a and b are constants (parameters of the material). The realisations differ in the definition of the state evolution law. Three well-known

Table 1
Summary of the different functional choices in (4) leading to common rate-and-state laws. The characteristic timescales of dynamic rejuvenation and quasistationary interfacial healing are $t_* = L/V_*$ and $t_{**} = Rt_*$, respectively. A state evolution kinetics of type $(4)_2$ is referred to as 'hyperbolic'.

Law	$\psi(\tilde{\phi})$	$\theta(\psi)$	$\psi_{ss}(\tilde{v})$	$t_\star(\tilde{v})$	ϕ_*	Kinetics
Dieterich	$\tilde{\phi}/\tilde{\phi}_*$	$\ln\psi$	$V_*/\tilde{v}$	$L/\tilde{v}$	t_*	First order
Generalised Dieterich	$\tilde{\phi}/\tilde{\phi}_*$	$\ln\psi$	$V_*/\tilde{v}$	$L/\tilde{v}$	t_*	Hyperbolic
Ruina	$\ln(\tilde{\phi}/\tilde{\phi}_*)$	ψ	$\ln(V_*/\tilde{v})$	$L/\tilde{v}$	t_*	First order
Perrin	$\ln(\tilde{\phi}/\tilde{\phi}_*)$	ψ	$\ln(V_*/\tilde{v})$	$L/\tilde{v}$	t_*	Hyperbolic
Spinodal	$\tilde{\phi}$	$\ln(c+\tilde{\phi}/\tilde{\phi}_*)$	$1/(1+Rv)$	$t_{**}\psi_{ss}(v)$	$1/(1+R)$	First order
Generalised spinodal	$\tilde{\phi}$	$\ln(c+\psi)$	$(1+R)/(1+Rv)$	$t_{**}/(1+Rv)$	1	Hyperbolic

[1] We use the term 'roughness' loosely since the link between the interfacial roughness and the magnitude of the friction coefficient is complex, for example smooth interfaces with a high microscopic contact area are able to generate high frictional forces.

choices for the state evolution law are

$$\begin{cases} d\tilde{\phi}/dt = 1 - \tilde{v}\tilde{\phi}/L & \text{(Dieterich/ageing law)},\\ d\tilde{\phi}/dt = -(\tilde{v}\tilde{\phi}/L)\ln(\tilde{v}\tilde{\phi}/L) & \text{(Ruina/sliplaw)},\\ d\tilde{\phi}/dt = 1 - [\tilde{v}\tilde{\phi}/(2L)]^2 & \text{(Perrinlaw)}. \end{cases} \tag{3}$$

Expressions (2)–(3) were originally proposed to embed three main experimental observations: (i) static friction increases logarithmically in time, (ii) in steady sliding, dynamic friction decreases logarithmically with increasing velocity, and (iii) sudden velocity jumps are observed to result in an adjustment of the dynamic friction coefficient which relaxes to the new value on a timescale intrinsic to the material. The diversity of proposed equations (3) reflects the choice and degree of detail retained by different models for interpretating experimental results in slide-hold-slide experiments (see e.g. Kato and Tullis, 2001). For instance, $(3)_1$ allows the prediction of the time-dependence of friction in stationary contact, while $(3)_2$ disregards this feature of stationary healing but accounts for the slip control of quasistationary friction strengthening (see Marone, 1998 for an exhaustive discussion with respect to experimental results). Nevertheless, we note that it is possible to propose a "composite state evolution law" which can resolve these drawbacks by adding to the right-hand-side of $(3)_2$ a velocity dependent quasistationary ageing term $\exp(-\tilde{v}/V_c)$, whose effect is therefore negligible for slip rates much larger than a velocity cut-off parameter V_c (see Kato and Tullis, 2001, 2003).

A common feature of these models, however, is that they all rely on the assumption that the interfacial state relaxes on a characteristic length scale L, independent of sliding velocity. This length is the so-called 'memory length' of the system, i.e. the distance over which the interface must slip before the effect of past variations in velocity on the current asperity population is lost. In this paper we challenge this point of view, as it seems to us more natural and general to introduce a relaxation timescale, rather than lengthscale, as we show below.

It is both interesting and instructive to observe that every one of the laws (2)–(3) can be derived from the pair of generic dimensionless expressions

$$\begin{cases} \mu = a\,\sinh^{-1}\left\{(v/2)\exp\left[(\mu_* + b\,\theta(\psi))/a\right]\right\},\\ d\psi/dt = -\sinh\left[\psi - \psi_{ss}(v)\right]/t_\star(v), \end{cases} \tag{4}$$

where $v \equiv \tilde{v}/V_*$ is a normalised velocity, $\psi := f(\tilde{\phi}/\tilde{\phi}_*)$ is a (similarly dimensionless) generic state variable possibly related to an empirical state variable $\tilde{\phi}$ [2], and $\theta(\psi)$ is a function describing the contribution of ψ to the friction coefficient μ. The form of $(4)_1$ can be derived from considering thermally activated Eyring rate processes which introduces the sinh function. Similar processes are also assumed here for the interfacial kinetics $(4)_2$, for which a first order differential equation is the usual form considered in the literature (e.g. see Putelat et al., 2011 and references therein). Interestingly, it has recently been proposed in Hulikal et al. (2015) that a first order kinetics for the interfacial state evolution is justified if the internal state variable ψ is defined to be the nth statistical moment of the friction force τ. In Putelat et al. (2011), we discussed both the derivation of such a general formulation for rate-and-state friction, and experimental procedures that might be able to confirm these functional forms, or support the use of others.

In order to complete the specification of a rate-and-state friction law within this formalism, we have to specify four components in (4):

- The functional form $\psi(\tilde{\phi})$ between the variable ψ and the underlying state variable $\tilde{\phi}$.
- The functional form $\theta(\psi)$ that captures the relationship between the friction coefficient μ and the state variable ψ.
- The functional form of $\psi_{ss}(v)$ which describes the steady-state (hence the subscript ss) relation between the state variable and the instantaneous slip velocity.
- The function $t_\star(v)$ that gives the effective timescale over which perturbations to the state variable relax to their equilibrium (i.e. steady-state sliding) value.

Two remarks are in order here. First, the first two components $\psi(\tilde{\phi})$ and $\theta(\psi)$ should be considered in combination since together they describe a change of coordinates that allows the treatment of different sets of assumptions about the thermodynamics and evolution of asperities on the microscale. Second, it is the dimensional homogeneity of (4) that first suggests the introduction of a timescale $t_\star$ describing the interfacial state kinetics. Contrary to the hypothesis that memory-length-controlled state relaxation has a constant timescale, the formulas (3) suggest that $t_\star$ certainly depends on the interfacial slip rate. It is quite possible that $t_\star$ depends also on the normal stress and the interfacial temperature. We leave the consideration of such additional complexity to future work.

We now consider each of the well-known friction laws in turn.

[2] As discussed in Putelat et al. (2011), the identification of a state variable with a precise physical process is a difficult task and still is a matter of debate. In that paper we showed in particular that different microphysical processes can lead to the same macroscopic functional form for the friction coefficient. In the absence of further physical evidence and a complete homogenised theory of friction, we prefer to view state variables as convenient mathematical tools for modelling the complex and incompletely known microscopic mechanisms at work during the sliding of rough interfaces.

Dieterich law

To derive the Dieterich/ageing law we make the following choices:

- $\psi = \tilde{\phi}/\tilde{\phi}_*$ where $\tilde{\phi}_* := L/V_*$ is a reference value of the timescale variable $\tilde{\phi}$. As mentioned above, L is the memory length and V_* is a characteristic slip rate for the system. Note that $\tilde{\phi}$ has dimensions of time and $\tilde{\phi}_*$ characterises the dynamic rejuvenation of the contact population,
- $\theta(\psi) = \ln \psi$ which describes the effect of surface roughness on the friction coefficient,
- $\psi_{ss}(v) = V_*/\tilde{v} = 1/v$ so that the steady-state value of the interfacial roughness decreases with increasing velocity, and
- $t_\star(v) = L/\tilde{v}$ the characteristic timescale for the interfacial state to adjust to changes in the slip velocity.

Note that L/V_* is an intrinsic timescale of the system even if other choices of relation between ψ and $\tilde{\phi}$ are made. We define $t_* = L/V_*$ and use t_* consistently to refer to this timescale throughout this section. Note that we could have written $t_\star(v) = t_* \psi_{ss}(v)$ linking the relaxation rate $t_\star$ to the steady-state value of the interfacial state. Substituting the above choices into the general form (4) and making two approximations (that $\sinh^{-1}(x) \approx \ln(2x)$ for large $x \gg 1$ in $(4)_1$, and that $\sinh(x) \approx x$ for $|x| \ll 1$ in $(4)_2$) we recover exactly the Dieterich law $(3)_1$. Note that μ takes its reference value μ_* exactly when $\tilde{v} = V_*$ and $\tilde{\phi} = \tilde{\phi}_*$.

If the approximation in $(4)_2$ is not made, we obtain a generalisation of the Dieterich law that will be useful for comparisons later; we refer to this system as the generalised Dieterich/ageing law:

$$\begin{cases} \mu = a \sinh^{-1}\left\{(v/2)\exp\left[(\mu_* + b\ln\psi)/a\right]\right\}, \\ d\psi/dt = -\sinh\left[\psi - \psi_{ss}(v)\right]/\left[t_*\psi_{ss}(v)\right], \end{cases} \tag{5}$$

where we note that $t_*\psi_{ss}(v) = (L/V_*)(V_*/\tilde{v}) = L/\tilde{v}$.

Ruina law

Similarly, a choice of functions that leads to the Ruina law is as follows:

- $\psi = \ln(\tilde{\phi}/\tilde{\phi}_*)$,
- $\theta(\psi) = \psi$,
- $\psi_{ss}(v) = -\ln(v) \equiv -\ln(\tilde{v}/V_*)$ so that again the steady-state value of the interfacial variable decreases with velocity, and
- $t_\star(v) = L/\tilde{v}$.

As for the Dieterich case, the further simplifying assumption in $(4)_1$ that $\sinh^{-1}(x) \approx \ln(2x)$ reduces the constitutive law to (2). The second assumption, that $\sinh(x) \approx x$ in the state evolution equation, implies that

$$\frac{d\tilde{\phi}}{dt} = -\tilde{\phi}\frac{\sinh\left[\ln(\tilde{\phi}/\tilde{\phi}_*) + \ln(\tilde{v}/V_*)\right]}{L/\tilde{v}} \approx -\frac{\tilde{v}\tilde{\phi}}{L}\ln\left(\frac{\tilde{\phi}\tilde{v}}{\tilde{\phi}_* V_*}\right) = -\frac{\tilde{v}\tilde{\phi}}{L}\ln\left(\frac{\tilde{v}\tilde{\phi}}{L}\right), \tag{6}$$

which is the usual form of the Ruina, or 'slip', law. Note that the relaxation rate $t_\star$ now takes the form $t_\star(v) = t_* \exp[\psi_{ss}(v)]$. The generalised form of the Ruina law, in which we do not make the approximation $\sinh(x) \approx x$ in the state evolution equation, is known as the Perrin law.

Perrin law

The Perrin law follows from the same collection of functional forms as specified for the Ruina law. A minor difference is that we specify the reference state of the state variable to be $\tilde{\phi}_* := 2L/V_*$ rather than L/V_*. Secondly, and more importantly, the evolution equation for the state variable is not linearised around the steady-state value as in (6). Instead we recall that $\sinh(\ln x) = \frac{1}{2}(x - 1/x)$ so that

$$\frac{d\tilde{\phi}}{dt} = -\frac{\tilde{v}\tilde{\phi}}{L}\frac{1}{2}\left(\frac{\tilde{v}\tilde{\phi}}{2L} - \frac{1}{\tilde{v}\tilde{\phi}/(2L)}\right) = 1 - \left(\frac{\tilde{v}\tilde{\phi}}{2L}\right)^2, \tag{7}$$

Thus the Perrin law is a generalisation of the Ruina law that exactly parallels the distinction between the generalised Dieterich law $(5)_2$ and the original Dieterich law $(3)_1$.

Spinodal law

The laws described above suffer from non-physical behaviour at both small and large velocities: the state variable either does not evolve at all at zero velocity (in the case of the Ruina law) or increases without bound (for the Dieterich law). At large velocities the interface becomes very smooth ($\tilde{\phi}$ becomes very small) and so the slip velocity increases unboundedly. In order to regularise the behaviour in these limits we introduced in previous papers (Putelat et al., 2007, 2011) a modification of the Dieterich law that (i) proposed that the state variable evolves in stationary contact (i.e. when $\tilde{v}=0$) to reach a characteristic interfacial strength of order unity, and (ii) proposed that the interface retains a residual strength c even at very high slip rates, thus avoiding unbounded acceleration at high velocities as in Weeks (1993). This regularisation effectively makes the velocity-dependence of the steady-state friction law $\mu_{ss}(\tilde{v})$ non-monotonic, with velocity-strengthening branches at low and high velocities and velocity-weakening behaviour over a range of intermediate velocities; the steady-state friction law thus exhibits a characteristic 'spinodal' N-shape.

The introduction of a finite maximum strength at low velocities implies the introduction of a new characteristic timescale t_{**} over which the interface relaxes towards this maximum value when $\tilde{v}=0$. This timescale t_{**} is distinct from both the characteristic timescale over which adjustments to the interfacial state take place as a result of velocity variations (this is $t_\star$), and from the timescale t_* which is based on the memory length L. On physical grounds we expect the ratio $R:=t_{**}/t_*$ to be much larger than unity.

Our spinodal law (Putelat et al., 2007, 2011) follows from the following choices:

- $\psi=\tilde{\phi}$,
- $\theta(\psi)=\ln(c+\tilde{\phi}/\tilde{\phi}_*)$,
- $\psi_{ss}(v)=1/(1+Rv)$,
- $t_\star(v)=t_{**}\psi_{ss}(v)$.

where we introduce the reference value of the interfacial state $\tilde{\phi}_*=1/(1+R)$ so that, as before, $\mu=\mu_*$ when $v=V_*$ in steady state. On substitution into the general formulation (4) we obtain

$$\mu=a\,\sinh^{-1}\left\{\frac{v}{2}\exp(\mu_*/a)\left(c+\tilde{\phi}/\tilde{\phi}_*\right)^{b/a}\right\},\quad\text{and}\quad\frac{d\tilde{\phi}}{dt}=-\frac{1+Rv}{t_{**}}\sinh\left[\frac{Rv\tilde{\phi}-(1-\tilde{\phi})}{1+Rv}\right],$$

which, on linearising by setting $\sinh x\approx x$, yields

$$d\tilde{\phi}/dt=(1-\tilde{\phi})/t_{**}-\tilde{v}\tilde{\phi}/L. \tag{8}$$

This form shows clearly the role of t_{**} as the characteristic timescale over which $\tilde{\phi}$ relaxes towards 1. Note that for this formulation the variable $\tilde{\phi}$ is in fact dimensionless rather than having the dimensions of time as in the Dieterich, Ruina or Perrin laws.

Although this spinodal law resolves several non-physical issues that are present in the Dieterich, Ruina and Perrin laws, it remains unsatisfactory in one respect that will be important for the particular problem we consider later in the paper: at low velocities, the evolution of the system is such that the interfacial velocity increases markedly while the interfacial state remains almost constant. This is counter-intuitive: at very low velocities we would expect the interfacial state to roughen towards its finite limiting value, and for the velocity to remain small.

Happily, this issue can be implemented through a slightly different formulation of the spinodal law: this is essentially a redefinition of the reference value of the interfacial state $\tilde{\phi}_*:=1$ and a compensating redefinition of the steady-state relationship $\psi_{ss}(v)$ so that $t_\star$ remains unchanged. We take

- $\psi=\tilde{\phi}$,
- $\theta(\psi)=\ln(c+\psi)$,
- $\psi_{ss}(v)=(1+R)/(1+Rv)$,
- $t_\star(v)=t_{**}\psi_{ss}(v)/(1+R)=t_{**}/(1+Rv)$.

Substitution into $(4)_1$ yields

$$\mu=a\,\sinh^{-1}\left\{(v/2)\exp\left[(\mu_*+b\ln(c+\tilde{\phi})/a\right]\right\}, \tag{9}$$

while substitution into $(4)_2$ yields

$$\frac{d\tilde{\phi}}{dt}=-\frac{1+Rv}{t_{**}}\sinh\left[\frac{Rv\tilde{\phi}-(1+R-\tilde{\phi})}{1+Rv}\right]. \tag{10}$$

Note that if we were to linearise the sinh function in the above expression, we would recover exactly (8). But in the nonlinear regime the behaviour differs in the two cases, and (10) has physically intuitive (and therefore preferable)

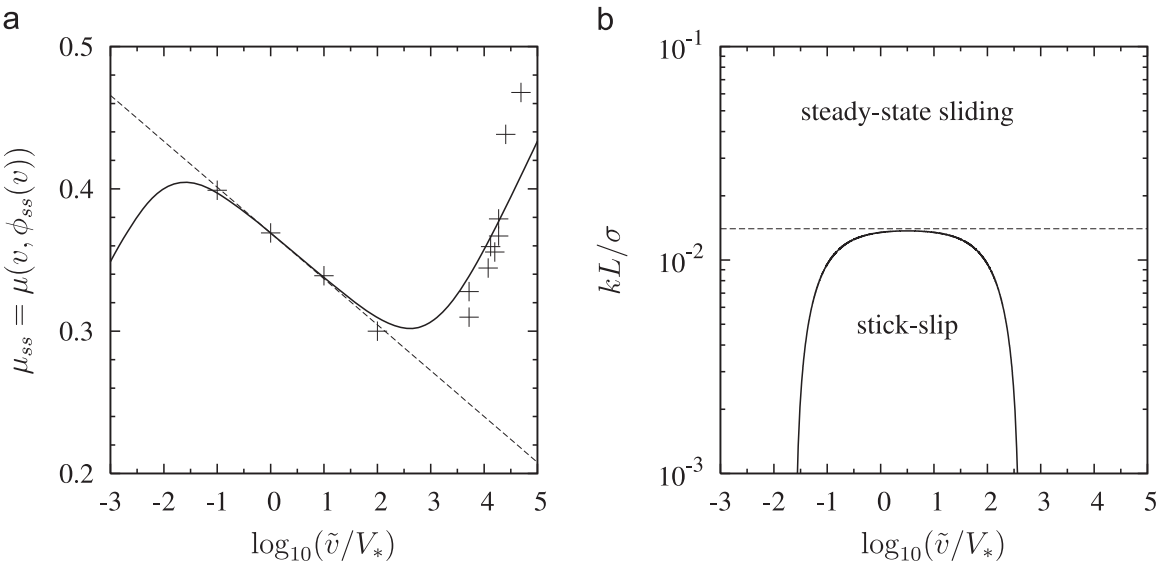

Fig. 1. Comparison of the Dieterich law (dashed lines) and spinodal law (solid lines) in steady state. Parameter values are as in Table 2. (a) Friction laws showing the value of the friction coefficient as a function of imposed sliding velocity. For the spinodal law we set $c=0.001$. The local maximum and minimum of the steady-state friction coefficient μ_{ss} are respectively located at $V_M = 2.49 \times 10^{-8}$ ms^{-1} and $V_m = 4.05 \times 10^{-4}$ ms^{-1}. The + symbols indicate experimental data from ref. Heslot et al. (1994). (b) Regime diagram for the dynamics of a block pulled horizontally at velocity $\tilde{v}$ by a spring of stiffness k, subject to a normal force σ, indicating the onset of stick-slip behaviour. For the Dieterich law $(3)_1$, stick-slip occurs below the dashed line; for the generalised spinodal law (10), stick-slip occurs only below the solid line.

behaviour at low velocities. Thus we will refer to the system (8) and (9) and as the 'spinodal law', and the system (9) and (10) as the 'generalised spinodal law'.

Analysis of the steady-state friction coefficient $\mu_{ss}(v) := \mu(v, \phi_{ss})$ computed by solving the state evolution equation for ϕ as a function of v indicates that $\mu_{ss}(v)$ takes the form shown in Fig. 1(a). There is a local maximum in $\mu_{ss}(v)$ at

$$V_M \approx aL/((b-a)t_{**}), \tag{11}$$

due to the competition between (quasi-)stationary interfacial strengthening controlled by the time scale t_{**} and dynamical weakening that takes place on the time scale $L/\tilde{v}$. The residual interfacial strength coefficient c produces a second turning point in $\mu_{ss}(v)$ where the velocity-weakening regime gives way to the high-velocity frictional strengthening branch. Hence there is a local minimum of $\mu_{ss}(v)$ at

$$V_m \approx (b/a-1)V_*/c. \tag{12}$$

We remark in passing that, for the classic mechanical problem of a block pulled horizontally by a spring of stiffness k across a frictional surface at a constant speed v, an important consequence of the existence of these local extrema in the steady-state friction law is to close up the domain of stick-slip sliding in the (V,k) parameter plane, see Fig. 1(b).

3. Sliding stability

In this section we use the rate-and-state friction framework of Section 2 to understand a specific elementary mechanical situation: the dynamics of a rigid block of mass m sliding on a flat plane inclined at an angle α to the horizontal, as shown in Fig. 2. The motion of the block is determined by two forces: the gravitational driving force $mg\sin(\alpha)$ and the resistive friction force $-mg\cos\alpha\mu(\tilde{v},\tilde{\phi})$. The dynamics is therefore given by Newton's Second Law coupled to the state evolution law, which we write in dimensional variables as

$$\begin{cases} \dot{\tilde{v}} = g\big[\sin\alpha - \mu(\tilde{v},\tilde{\phi})\cos\alpha\big], \\ \dot{\tilde{\phi}} = -G(\tilde{v},\tilde{\phi}). \end{cases} \tag{13}$$

It is obvious from $(13)_1$ that the block slides downward in steady state with a velocity $\tilde{v}=V$ and an interfacial state $\tilde{\phi}=\tilde{\phi}_{ss}(V)$ that are determined by the angle α. V and $\tilde{\phi}_{ss}(V)$ are solutions of the pair of

$$\mu_{ss}(V,\tilde{\phi}_{ss}) = \tan\alpha, \quad \text{and} \quad G(V,\tilde{\phi}_{ss}(V)) = 0.$$

The growth rates s of infinitesimal perturbations to the velocity and the interfacial state of the steady state $(V,\tilde{\phi}_{ss}(V))$ are

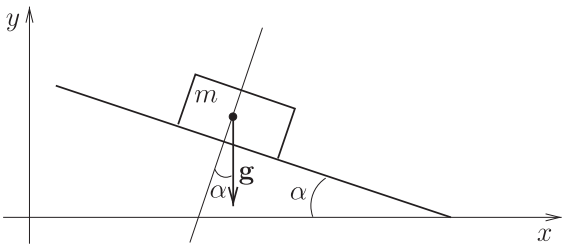

Fig. 2. A block sliding on a slope. Slow increments in the angle α allow the naive determination of a critical 'angle of friction' α_c at which the block first begins to move.

given by the eigenvalues of the Jacobian matrix of (13) evaluated at $(V, \tilde{\phi}_{ss}(V))$. This yields the characteristic equation

$$s\left[s + G_\phi + g\cos\alpha\mu_v\right] = -g\cos\alpha G_\phi \mu_{ss}'. \tag{14}$$

We denote the slope of the steady-state friction coefficient evaluated at $v=V$ by the total derivative $d\mu_{ss}/dv \equiv \mu_{ss}'$. We denote the partial derivatives of the functions G and μ with respect to $\tilde{\phi}$ and v by G_ϕ and μ_v; these are assumed further to be the values evaluated at the steady state $(V, \tilde{\phi}_{ss}(V))$. As previous authors have commented, we suppose that the partial derivatives G_ϕ and μ_v are positive, in agreement with observations (Rice et al., 2001). Plotting the left-hand side of the characteristic equation (14) graphically shows that one of the growth rates is positive when $\mu_{ss}' < 0$. Therefore, the steady-state sliding of the block is unstable for slip rates which correspond to a velocity-weakening branch of the friction coefficient.[3] In other words, the equilibrium point $(V, \tilde{\phi}_{ss}(V))$ of (13) is a saddle point in this regime, whereas it is a stable node in regimes for which friction is velocity-strengthening (i.e. $\mu_{ss}'(V) > 0$)[4].The change in the nature of the steady-state sliding, from stable node to saddle point, suggests that a saddle-node bifurcation occurs at slip rates V at which the slope of the steady-state friction coefficient $\mu_{ss}(V)$ changes sign.

We remark briefly that analyses of exactly this kind have been carried out, using the monotonic Ruina law, in order to understand the dynamics of landslides, see Chau (1995), Chau (1999), and Helmstetter et al. (2004).

3.1. Sliding dynamics with the spinodal law

As the discussion at the end of Section 2 indicates, we expect two saddle-node bifurcations to take place when we adopt the spinodal law (9)–(8) or its generalised form (9)–(10). In this section the choice of the linearised, or generalised form is immaterial since we study only the steady-state sliding dynamics. The velocities at which the saddle-node bifurcations occur are close to the approximate values (11) and (12). Physically, as we now discuss, it makes sense to associate the bifurcation at $V = V_M < V_m$, at which there is a local maximum in the steady-state friction curve, with the notion of a static friction coefficient. Consider the thought experiment in which we slowly increase the angle α starting from the horizontal. We imagine that this is performed quasi-statically so that steady-state sliding (i.e. at constant velocity) is reached after each increment of α. In such a case, the block slides with extremely low velocities $V < V_M$ that increase very slowly with α until the angle attains the critical value α_{cM} that is given by the relation $\tan\alpha_{cM} = \mu_{ss}(V_M)$. For angles $\alpha > \alpha_{cM}$, the constant velocity state is linearly unstable and the block accelerates rapidly. Therefore, the static friction coefficient μ_s measured in such an experiment corresponds to the value of μ at the local maximum of the steady-state friction law:

$$\mu_s = \tan\alpha_{cM} = \mu_{ss}(V_M). \tag{15}$$

Hence both the static friction coefficient μ_s and the angle of internal friction α_{cM} can be expressed in terms of the material parameters involved in the friction law (10). Numerically, using the estimate $V_M = 2.49\times10^{-8}\ \mathrm{ms}^{-1}$ given by (11), we find $\alpha_{cM} \approx 0.385$ rad $\approx 22°$. To summarise, the empirical observation that there exists a critical angle at which a block starts sliding on an inclined plane corresponds directly to the existence of a local maximum in the steady-state form of a rate-and-state friction law. In this formalism the interpretation is that for angles smaller than the angle of internal friction α_{cM}, the block creeps down so slowly that an impatient human eye does not notice it. For a block sliding steadily at about $10^{-2}V_* \equiv 10^{-8}\ \mathrm{ms}^{-1}$, around 1.2 days would be necessary for the block to slip by a distance of 1 mm; to slip by 1 mm at a velocity of $10^{-3}V_* \equiv 10^{-9}\ \mathrm{m\,s}^{-1}$ would take around 12 days.

Further, the local minimum $\mu_{ss}(V_m)$ and maximum $\mu_{ss}(V_M)$ for the spinodal law define a range of angles

$$\alpha_{cm} \equiv \tan^{-1}\left[\mu_{ss}(V_m)\right] \le \alpha \le \tan^{-1}\left[\mu_{ss}(V_M)\right] \equiv \alpha_{cM}, \tag{16}$$

bounded by the saddle-node bifurcations that occur at (α_{cm}, V_m) and (α_{cM}, V_M) according to the elementary stability analysis

[3] Note that if the friction coefficient were a function of the slip rate only, the growth rates of the perturbation would be $-g\cos\alpha\mu_{ss}'(V)$ which leads to the same conclusion.

[4] The remaining generic possibility, that of a stable focus, cannot in fact occur in (13).

above. Between the saddle-node bifurcations lies a domain of bistability where two linearly stable steady-state slidings coexist, along with a third (unstable) steady-state sliding solution.

This is illustrated in Fig. 3 which shows the branch of the steady-state solution of (13) as the parameter α varies.

We computed the location of the critical angles α_{cm} and α_{cM} as the residual strength parameter c varies, using the continuation software AUTO (Doedel et al., 1991). Fig. 4 shows that the region of bistability closes as c increases so that the system is not bistable for c sufficiently large, and it expands as c decreases. The residual strength of the frictional interface is thus an essential ingredient of the problem. Fig. 4 indicates clearly that, for the range of 'dangerous' slope angles $\alpha_{cm} \le \alpha \le \alpha_{cM}$, the upper limit α_{cM} is almost independent of c – it corresponds to the position of the local maximum in $\mu_{ss}(V)$ at low velocities $V \approx V_M$. The lower limit α_{cm} varies strongly with c, in fact it varies almost linearly with $\ln c$ until it saturates at very small c; α_{cm} depends on the location of the local minimum V_m at which the high velocity regime turns from velocity-weakening to velocity-strengthening at higher velocities.

Although Fig. 3 is computed using the particular friction law (10) its geometrical shape is generic for any steady-state spinodal law. Interestingly, the presence of the saddle point in the bistability domain makes both stable solutions unstable to sufficiently large finite amplitude perturbations in either velocity V or interfacial state ϕ. An approximation to the order of magnitude of such perturbations that would be required to kick the system into the other steady state is given (geometrically) by the form of the friction law as shown in Fig. 1(a) or by the curves in Fig. 3. Quantitatively, within the velocity-

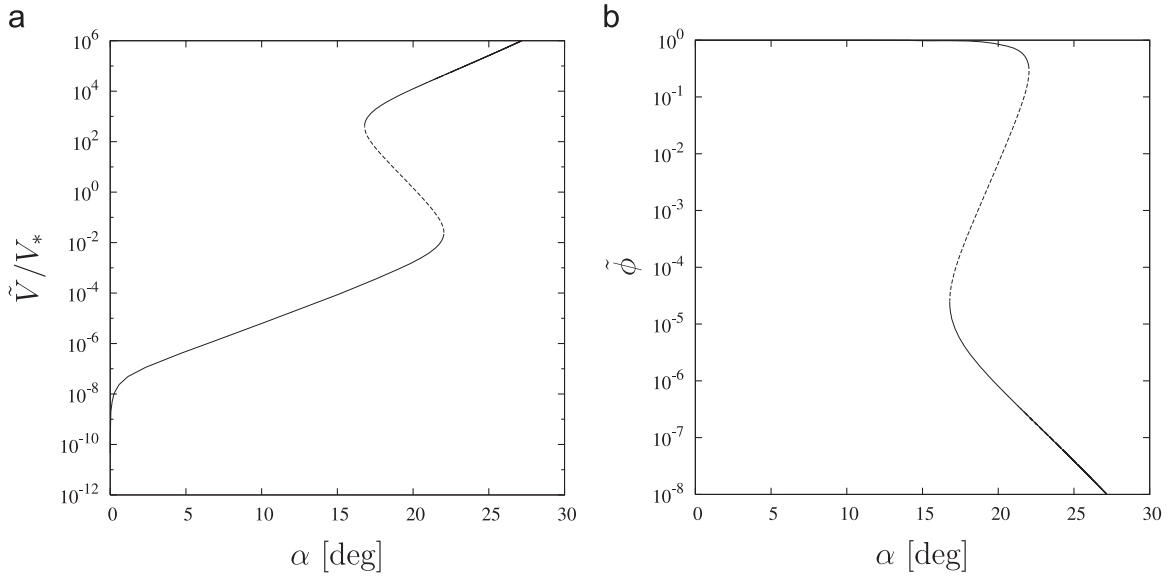

Fig. 3. Bifurcation diagram showing steady sliding solutions of the sliding block system (13) using the spinodal law. For slope angles α such that $\alpha_{cm} \le \alpha \le \alpha_{cM}$, three steady-state sliding velocities are possible. Solid and dashed lines represent stable and unstable solutions, respectively. The critical angles α_{cm} and α_{cM} are determined by the local extrema of the steady-state friction coefficient, see (16).

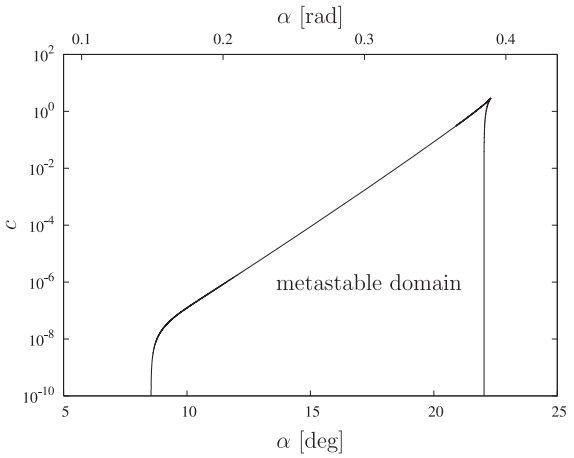

Fig. 4. Region of bistability in the (α, c) plane for the sliding block system (13) using the spinodal law (9)–(10). Within the region marked 'metastable domain' there are two stable sliding solutions.

weakening regime, the spinodal law (10) is extremely close to the Dieterich law (2)–$(3)_1$ so that the friction coefficient can be well approximated by (2): to be precise, in steady state we have $\mu \equiv \mu_{ss}(V) = \mu_* + (a-b)\ln(\tilde{v}/V_*)$ so setting $\mu = \tan\alpha$ and rearranging we see that the required amplitude of velocity perturbations would be of the order of $V_* \exp\left[(\mu_* - \tan\alpha)/(b-a)\right]$, for angles α in the range $\alpha_{cm} \le \alpha \le \alpha_{cM}$. The size of this perturbation varies strongly with α near V_*: this variation is connected to the fast variation of the exponential term which in turn is due to the difference between the two parameters a and b being relatively small: $b - a = O(10^{-2})$.

To go further it is necessary to examine the details of the phase portrait of the dynamical system (13) and to investigate the topological changes in the phase portrait that are implied by the bifurcation diagram in Fig. 3. Fig. 5 presents a typical phase portrait for the spinodal law (10) for a slope angle $\alpha = 0.34$ rad $\approx 19.5°$ inside the interval of bistability. As shown in the figure, the two stable nodes and the saddle point are located at the three intersections of the $\tilde{v}$ and $\tilde{\phi}$ nullclines. The $\tilde{\phi}$-nullcline ($\dot{\tilde{\phi}} = 0$) is fixed in the $(\tilde{v}, \tilde{\phi})$ phase plane and coincides with the equilibrium interfacial state $\phi = \phi_{ss}(V)$: it is therefore purely a property of the interface. In contrast, the location of the $\tilde{v}$-nullcline ($\dot{\tilde{v}} = 0$) depends on the slope angle α. As α is increased quasi-statically the $\tilde{v}$-nullcline is displaced towards larger values of $\tilde{v}$. As a result, we can see geometrically that when $\alpha < \alpha_{cm}$, the $\tilde{v}$-nullcline intersects the $\tilde{\phi}$-nullcline only at low velocity and high interfacial state, and when $\alpha > \alpha_{cM}$ the $\tilde{v}$-nullcline intersects the $\tilde{\phi}$-nullcline only at high velocity and low interfacial state. These intersections between nullclines are the stable branches of steady states shown in Fig. 3.

For $\alpha_{cm} \le \alpha \le \alpha_{cM}$ the presence of the saddle point divides the phase plane in two basins of attraction separated by the stable manifold of the saddle point. If initial conditions are chosen in the upper left corner of the phase plane, above the stable manifold, then the block will creep down the slope at a very slow rate, essentially stopping. This corresponds to interfaces that are rough, and slowly moving. In the other basin of attraction, the block will accelerate until reaching the high-velocity steady state associated with a smooth interface.

3.2. Sliding dynamics with the Dieterich law

In this section we make brief remarks to compare the description of the dynamics when the Dieterich law (which has a monotonically decreasing steady-state friction coefficient $\mu_{ss}(V)$) is used to that resulting from the spinodal law. The deficiencies that we identify in the Dieterich law are remedied by the spinodal law; this discussion serves to clarify and justify the preceding section and the use of the spinodal law.

Fig. 6(a) presents the phase portrait of the sliding block system (13) using the Dieterich law $(3)_1$. There is exactly one equilibrium point (a saddle point) for all slope angles α due to the monotonic character of $(3)_1$. The stable manifold of the saddle point divides the phase plane into two regions, similar to its role in the spinodal law (10) for angles in the bistable regime.

For the Dieterich law, starting at an initial condition in the region above the stable manifold in Fig. 6(a) leads to the block slowing down indefinitely; for initial conditions in the region below the stable manifold, the block accelerates without bound. As a result, the definition of a static coefficient of friction that we motivated for the non-monotonic friction law in the subsection above cannot be used here.

The only possible mechanism that allows for a sudden transition to rapid slip as the angle α increases is to say that, since the saddle point is displaced towards low velocities and higher interfacial state values as the slope angle is increased, there must be a point at which the interfacial state and the instantaneous (low) velocity of the block crosses through the stable manifold of the saddle point, since the stable manifold of the saddle moves when the saddle point itself moves. Such a

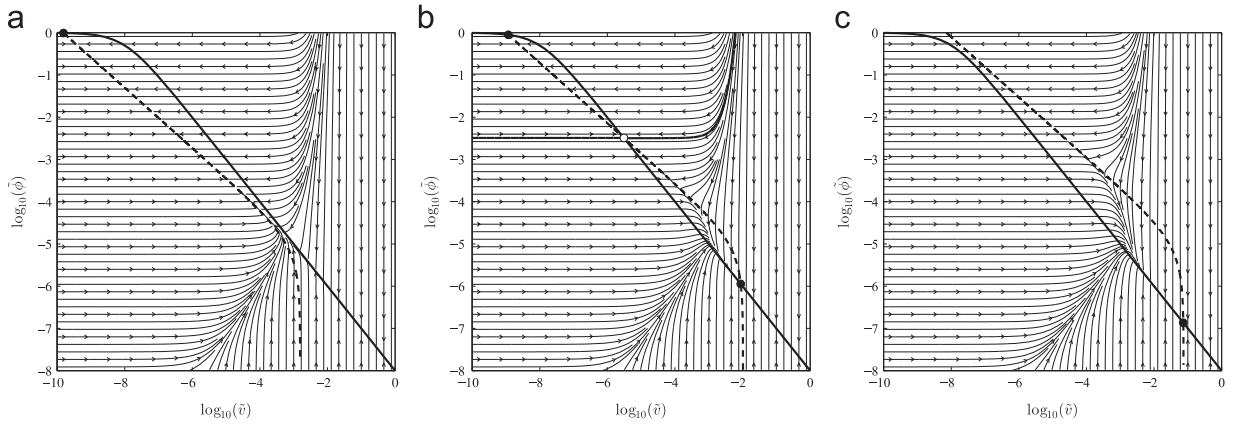

Fig. 5. Phase portrait in the $(\tilde{v}, \tilde{\phi})$ plane for the system (13) that describes a block sliding on a slope of angle α. (a) $\alpha = 0.28$; (b) $\alpha = 0.34$ rad $\approx 19.5°$; (c) $\alpha = 0.4$. In each plot the nullclines $\dot{v} = 0$ and $\dot{\phi} = 0$ of (13) are indicated by the thick dashed and solid lines, respectively. The solid line is the locus of steady-state sliding $\phi = \phi_{ss}(v)$; the stable nodes are indicated by solid dots ● and the saddle point is indicated by the white dot ○. Thin lines with arrows are trajectories of (13). Thick lines indicate the stable manifold of the saddle point: note that these curves divide the phase plane into two separate basins of attraction. Initial conditions in the upper (*resp.* lower) region lead to "stopping" (*resp.* "sliding") motion of the block: (a) $\alpha = 0.28$; (b) $\alpha = 0.34$; (c) $\alpha = 0.40$

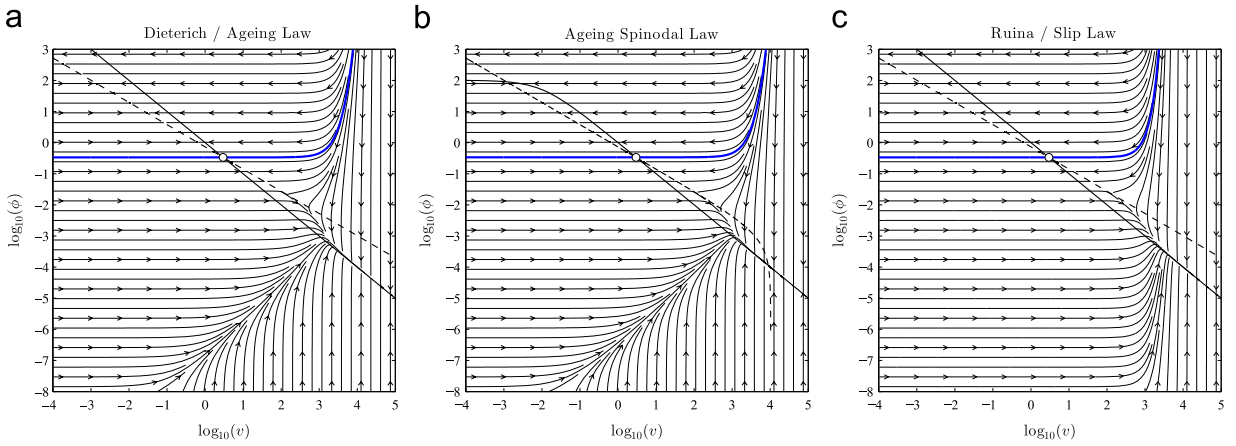

Fig. 6. Phase portraits of the sliding block system under different rate-and-state friction laws, using the 'first order kinetics' approximation, linearising the state evolution law near the steady-state response $\psi_{ss}(v)$. The slope angle α is fixed at $\alpha = 0.34$. (a) Dieterich law (3); (b) spinodal law (8); (c) Ruina law (6). On each plot, the v-nullcline and the ϕ-nullcline correspond respectively to the thick dashed line and the thick solid line. On the v-nullcline, the instantaneous friction coefficient satisfies $\mu(v, \phi) = \tan\alpha$. The stable manifold of the saddle point is given by the solid (blue) line that extends from lower left to top right on each plot. (For interpretation of the references to color in this figure caption, the reader is referred to the web version of this article.)

sudden transition can be achieved if the slope angle is varying fast enough. However, since any critical angle defined according to the above argument depends on the interfacial state of the block, we might expect that such a criterion would inevitably lead to scatter in experimentally recorded measurements of the value of the static friction coefficient.

Taking a global view, the facts that the saddle point and its unstable manifold persist over the full range of α from 0° to 90° and that the low-velocity branch of the stable manifold of the saddle point appears not to extend to small values of $\tilde{\phi}$, implies that unbounded accelerations of the block are always possible if the interface is sufficiently smooth. This unphysical feature of the dynamics is removed by modifying the friction law to contain a velocity-strengthening branch at high velocities. As remarked on in the previous section, modifying the Dieterich law in this way allows the definition of a static friction coefficient, associated with the local minimum of the steady-state friction coefficient. Conversely, the persistence of the saddle point and its stable manifold implies also that, if the interface is sufficiently rough, the block will remain at rest (i.e. move imperceptibly slowly) for any slope angle, even very large ones. This observation suggests that it is necessary also to include a velocity-strengthening branch at very low velocities, in order to force the disappearance of the saddle point, and with it the basin of attraction of the rest state, above a critical angle α_{cM}.

3.3. Phase portraits for different friction laws

In this subsection we briefly present phase portraits for the dynamics of the sliding block problem when each of the different rate-and-state friction laws is used. The results are summarised in Figs. 6 and 7. Fig. 6 presents three phase

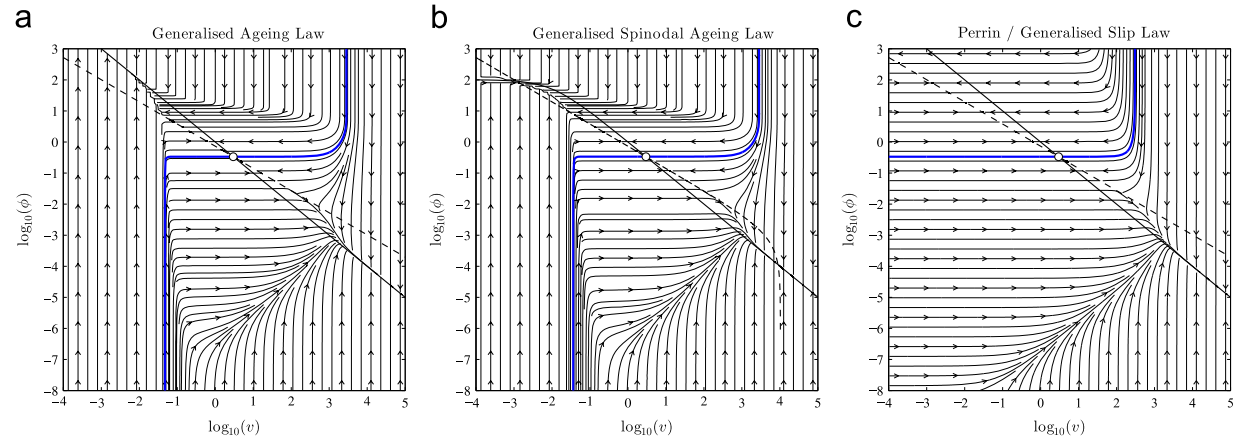

Fig. 7. Phase portraits of the sliding block system under different rate-and-state friction laws, using the fully nonlinear state evolution laws. The slope angle α is fixed at $\alpha = 0.34$. (a) Generalised Dieterich law (5); (b) generalized spinodal law (10); (c) Perrin law (7). On each plot, the v-nullcline and the ϕ-nullcline correspond respectively to the thick dashed line and the thick solid line. On the v-nullcline, the instantaneous friction coefficient satisfies $\mu(v, \phi) = \tan\alpha$. The stable manifold of the saddle point is given by the solid (blue) line that extends from lower left to top right on each plot. (For interpretation of the references to color in this figure caption, the reader is referred to the web version of this article.)

portraits for the Dieterich (3), spinodal (8), and Ruina (6) laws: in every case the state law is linearised around the steady-state friction law. Fig. 7 presents the corresponding phase portraits for the three cases when the fully nonlinear state evolution laws are used instead of their linearisations. The phase portraits summarise clearly the similarities and important differences between the six cases.

The stable manifold of the saddle point (indicated on each figure by a solid (blue) line) divides the phase portrait into two regions. For initial conditions (v_0, ϕ_0) above the stable manifold, the block ultimately slows down and in most cases is attracted to the v-nullcline (dashed line) on which $\mu(v, \phi) = \tan(\alpha)$. For initial conditions below the stable manifold, in the cases of the Dieterich and the Ruina laws with first-order kinetics (Fig. 6(a) and 6(c)) the block continues to accelerate since trajectories are attracted to the ϕ-nullcline on which $\mu = \mu_{ss}(v) < \tan(\alpha)$. For the spinodal laws in Figs. 6(b) and 7(b), trajectories starting below the stable manifold of the saddle are eventually attracted to a stable node corresponding to high-velocity sliding.

As the slope angle is increased, the saddle node moves leftwards and the size of the region of the phase plane in which the block eventually stops is reduced. For cases in which the friction law is monotonically velocity-weakening (i.e. Figs. 6(a,c) and 7(a,c)), the concepts of static friction coefficient and critical angle of stability can then be interpreted as the stable manifold crossing the initial condition of the block. As we have already remarked, the laws illustrated in Fig. 6 are unphysical in that, even for small slope angles, acceleration is admitted for very smooth interfaces ($\phi \ll 1$). This possibility motivates the need to allow frictional velocity-strengthening at high speed.

We turn now to the fully nonlinear 'generalised' forms of the friction laws. The inclusion of the full nonlinear form of the state evolution law in the Dieterich and spinodal models, see Figs. 7(a) and 6(b), has the effect of bending the stable manifold of the saddle towards lower values of ϕ at low v. This creates a region at low speed that is always 'above' the stable manifold of the saddle in the sense that the interface strengthens without the velocity increasing. This behaviour mimics the behaviour of 'Coulomb friction' at zero velocity. In Fig. 7(a) trajectories above and to the left of the stable manifold of the saddle are attracted first to the v-nullcline near the saddle, before being attracted to the ϕ-nullcline further away. The phase portrait, Fig. 7(c), for the Perrin law (7) closely resembles that obtained for the (linearised) Dieterich law, see Fig. 6(a).

To summarise, in this section we have highlighted the existence of two distinct regions in the phase plane, and the role played by the stable manifold of the saddle point as the boundary between them. In the next section we use this interpretation of the dynamics to shed light on the behaviour found experimentally by Rabinowicz (1951) and quantitatively to connect informal ideas of 'static' and 'dynamic' friction coefficients with the rate-and-state formalism.

4. Rabinowicz's impact experiments

In this section we discuss the experiments reported by Rabinowicz (1951) and show that his results can be interpreted as an experimental exploration of the phase portrait of the sliding block. This implies that experimental measurements of the dynamical behaviour can be used to produce a quantitative estimate of the memory length L. To begin with, in Section 4.1 we summarise the experimental setup and reasoning given by Rabinowicz before interpreting it within the rate-and-state framework. The behaviour in Rabinowicz's experiment is described in terms of two separate phases. The first of these provides a surprisingly clear link between the persistence length that he introduced, and which we define below, and the parameters of the rate-and-state laws. This is described in Section 4.2. A third, final, phase exists for choices of the friction law that contain an attracting stable equilibrium point (for example the spinodal law). In Section 4.4, we discuss the different phases of the dynamical behaviour in terms of trajectories in the phase portrait.

Starting from the dimensional equations of motion (13), we nondimensionalise lengths and times using the memory length L and the asperity dynamic rejuvenation time $t_* = L/V_*$. We use the generalised spinodal law (9)–(10) and so derive the dimensionless dynamical

$$\begin{cases} \epsilon^2 \dot{v} = \sin\alpha - \cos\alpha\, \mu(v, \psi), \\ \eta\, \dot{\psi} = -\sinh[\psi - \psi_{ss}(v)]/\psi_{ss}(v), \end{cases} \tag{17}$$

where the dots represent differentiation with respect to the dimensionless time t and the friction coefficient $\mu(v, \psi)$ is given by (9) (recall we set $\psi = \tilde{\phi}$). ϵ and η are dimensionless parameters defined as follows:

$$\epsilon := \sqrt{L/g}\,/(L/V_*), \quad \text{and} \quad \eta := R/(1+R). \tag{18}$$

With L as the reference length, ϵ indicates the relative magnitude of the free fall time $\sqrt{L/g}$ compared to the interfacial dynamic rejuvenation time L/V_*. For typical values of the memory length $L \sim 10^{-6}$ m and the reference velocity $V_* \sim 10^{-6}$ ms^{-1}, ϵ is around 10^{-4}. Recall that $R = t_{**}/t_*$ is the ratio of the interfacial relaxation time (in quasi-stationary contact) t_{**} to the time t_* derived from the memory length L. We expect $R \gg 1$ and therefore η is expected to be close to unity. As before, for the generalised spinodal law we have $\psi_{ss}(v) = (1+R)/(1+Rv)$.

4.1. The experimental setup

Rabinowicz's experiments study how far a block of mass m, which is initially at rest, slides on a planar slope after the block is impacted by a rolling spherical ball of mass $m_b \ll m$. The impulse is generated by allowing the rolling spherical ball to travel a distance l, also starting from rest, before the impact with the block. The impact of the ball on the block then accelerates the block down the slope. The principal parameters varied in the experiments are therefore the slope angle α and the distance l between the point of release of the ball and the initially stationary block.

Rabinowicz began from the classic idea that there are two constant friction coefficients: the static value μ_s required to initiate the motion of the block, and the kinetic value $\mu_k < \mu_s$ that retards the motion while the block slips. Rabinowicz fixed α so that $\mu_k < \tan\alpha < \mu_s$ and performed experiments in which the release distance l is varied. He observed that there exists a critical length l_k below which the block creeps down only a small distance (of the order of 10^{-4} cm) until it comes to rest, and above which the block is set into 'large-amplitude' motion down the slope.

In order to explain these results, the simplest model, as proposed by Rabinowicz, is to assume a slip-dependent piecewise constant friction coefficient $\mu(s)$, i.e. that $\mu(s) = \mu_s$ for $0 \le s < s_k$ and $\mu(s) = \mu_k$ for $s > s_k$. He referred to the distance s_k at which this fast drop in the friction coefficient occurs as the 'persistence length'. If the kinetic energy transferred to the block from the ball is not sufficient to make the block slide a distance s_k then the block will stop; if the kinetic energy supplied to the block is sufficient to allow longer slip then the block would continue sliding for a distance greater than s_k.

The relation between the persistence length s_k and the corresponding critical release distance l_k of the ball is given by elementary mechanics, as follows. Conservation of energy implies that the distance s over which the block slips before coming to rest is given by

$$g(\mu_s \cos\alpha - \sin\alpha)s = v_0^2/2, \tag{19}$$

where v_0 denotes the initial block velocity just after the impact of the rolling ball. Assuming that the transfer of momentum during impact can be characterised by a coefficient of restitution e that relates the velocity v_b of the ball to v_0 we have the relation

$$mv_0 = (1+e)m_b v_b. \tag{20}$$

The velocity v_b of the ball at impact is similarly determined energetically, assuming that it rolls without slipping over the distance l from the initial point of release. Recalling the moment of inertia of a sphere about its contact point with a tangent plane we have the relation

$$v_b^2 = (10/7)gl\sin\alpha. \tag{21}$$

Combining (19), (20) and (21) gives the slip distance s for the block (in the regime where it is at most s_k) in terms of the release distance of the ball, l:

$$(\mu_s - \tan\alpha)s = Kl\tan\alpha, \tag{22}$$

where, for notational simplicity, we have defined the constant $K = (5/7)(1+e)^2(m_b/m)^2$. Experimental determinations of the critical release distance l_k then lead directly to estimates for the persistence length s_k: $(\mu_s - \tan\alpha)s_k = Kl_k\tan\alpha$.

In reality, the variation of the friction coefficient with distance from rest will not be piecewise constant as in Fig. 8(a). In order to deduce experimentally the true form of the μ–s curve, Rabinowicz modifies the above argument slightly, as follows. For a friction coefficient μ that varies with distance s, we have the straightforward generalisation of (22):

$$\int_0^s \mu(s')\,ds' - s\tan\alpha = Kl\tan\alpha, \tag{23}$$

between the release height l and the slip distance s. Since the left-hand side is equal to $\int_0^s \mu(s') - \tan\alpha\,ds'$ we must have that the slip distance s_k at which the block stops is given by the constraint that $\mu(s_k) = \tan\alpha$, since $\mu(s) > \tan\alpha$ for $0 \le s < s_k$ in order to place the block in motion initially. So in general we have

$$\int_0^{s_k} \mu(s') - \tan\alpha\,ds' = Kl_k\tan\alpha, \tag{24}$$

Moreover, since the block is monotonically decelerating over the whole time it is in motion, the friction force is monotonically decreasing. This implies that we can re-express the integral on the left-hand side of (24), using also the fact that $\mu(0) = \mu_s$, as

$$\int_0^{s_k} \mu(s') - \tan\alpha\,ds' \equiv \int_{\tan\alpha}^{\mu_s} s(\mu')\,d\mu'.$$

Substituting this into (23) gives

$$Kl_k\tan\alpha = \int_{\tan\alpha}^{\mu_s} s(\mu')\,d\mu'.$$

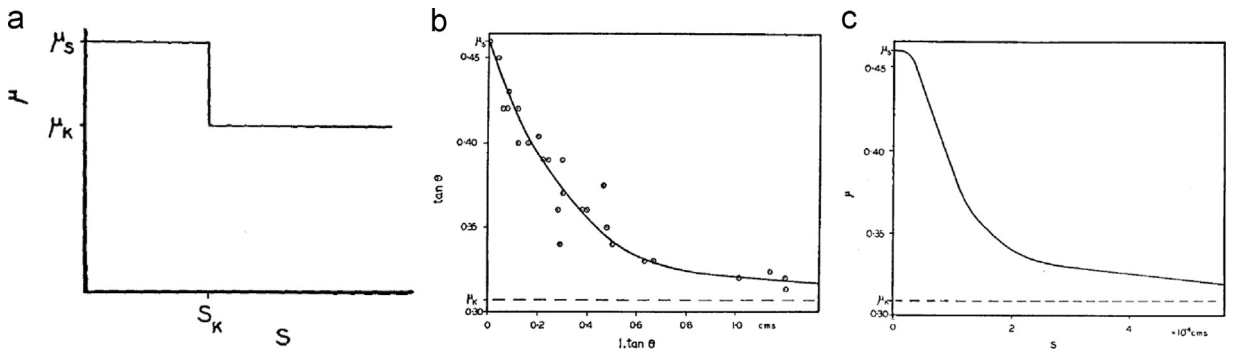

Fig. 8. Figures reproduced from Rabinowicz (1951). (a) Illustrative sketch of the piecewise-constant friction coefficient μ as a function of the persistence length s. The friction coefficient is proposed to take the static value μ_s over slip distances $0 \le x \le s_k$ and the lower (kinetic) value μ_k for $x > s_k$. (b) Experimental data (points) and smoothed average (solid curve) of $\tan\alpha$ (vertical axis) as a function of $l\tan\alpha$ (horizontal axis). Data were obtained for a copper upper surface sliding down a steel slope. (c) Friction coefficient $\mu(s)$ inferred from the plot in (b); μ is proportional to the negative of the reciprocal of the derivative of the curve in (b).

Despite the slightly convoluted manipulations, this relation is just a different representation of the energy balance as the block moves. Differentiating with respect to $\tan\alpha$, we obtain the relation

$$-K\frac{d(l_k\tan\alpha)}{d(\tan\alpha)} = s(\tan\alpha) =: s_k. \tag{25}$$

This indicates that the plot of the friction coefficient $\mu(s_k)$ as a function of the critical slip distance s_k can be obtained by plotting $\tan\alpha$ (since $\tan\alpha = \mu$ exactly when $s = s_k$) as a function of $-K\ d(l_k\tan\alpha)/d(\tan\alpha)$, as this expression is equal to s_k. We illustrate this in Figs. 8(b) and (c) with images from Rabinowicz's original paper (Rabinowicz, 1951). We refer the interested reader to this paper for details of the experimental setup. Fig. 8(b) shows experimental data for $\tan\alpha$ (on the y-axis) against $l_k\tan\alpha$ (on the x-axis). The reciprocal of the negative of the gradient of the solid curve is therefore s_k and the corresponding estimated plot of $\mu(s_k)$ against s_k is shown in Fig. 8(c).

In the next two subsections we discuss, using the generalised Dieterich ageing law (5) to be specific, how we can interpret this behaviour in terms of the smooth rate-and-state description of friction. The idea of the persistence length s_k is very attractive since it is a straightforward macroscopic quantity than can be measured in the laboratory. We consider the evolution starting from different initial conditions: a rough interface with a block moving at high velocity, then a smooth interface with a block moving slowly. We note that our conclusions from the block experiment should apply also to frictional interfaces dividing continua when spatial variations are ignored, or assumed to arise only on long wavelengths. Finally, in this section, we discuss the long-time evolution close to equilibrium when a spinodal law is used to regularise the behaviour at low velocities by providing a velocity-strengthening branch to the friction law that prevents the interface becoming infinitely rough.

4.2. Analysis starting from a rough, high velocity initial condition

Starting from a (dimensionless) initial condition (ψ_0, v_0) in which the interface is rough and for which a large initial impulse is applied to the block, so that ψ_0 and v_0 are both large, it is straightforward to estimate the total distance x that the block slips before coming to rest. As we remarked before, the stable manifold of the saddle point divides the phase portrait into cases in which the block ultimately stops and cases in which it accelerates unboundedly, if no high-velocity residual frictional strength is introduced. To estimate the rate-and-state persistence length, we consider initial conditions that are very close to the stable manifold, in the upper right-hand corner of the phase portraits shown in Figs. 6 and 7.

When $\psi_0 \gg \psi_{ss}(v_0)$ (recall that $\psi_{ss}(v)$ denotes the steady-state value of $\psi(v)$ at constant velocity v), we may approximate the state evolution law $(17)_2$ by

$$\eta\,\dot{\psi} = -\ \sinh(\psi)/(1/v),$$

since $\psi_{ss}(v) = (1+R)/(1+Rv) \approx 1/v$. This can be integrated with respect to time immediately to give

$$x(t) = \int_0^t v(t')\,dt' = \eta\,\ln\left[\tanh(\psi_0/2)/\tanh(\psi(t)/2)\right]. \tag{26}$$

This shows that, to leading order, the slip distance $x(t)$ is determined by the state variable during the fast initial phase of deceleration. Interestingly, for the Dieterich law, (26) would read $x(t) = -\ \ln(\psi/\psi_0)$, which suggests an interpretation of the $\ln\psi$ term in the friction law (2) as the slip distance over which the instantaneous friction coefficient is reduced to its kinetic value, as set by $\tan\alpha$.

Multiplying $(17)_1$ by v and time-integrating up to the point at which the block comes to rest, we obtain

$$-\frac{\epsilon^2}{2}v_0^2 = \sin\alpha \int_0^{t_{rest}} v\, dt' - \cos\alpha \int_0^{t_{rest}} v\mu\, dt' \tag{27}$$

Comparison with Rabinowicz's expression (19) results in the following relation, which provides a *definition* of the static friction coefficient μ_s as a weighted average of the rate-and-state friction coefficient over the block motion:

$$\mu_s := \int_0^{t_{rest}} \mu(t')v(t')\, dt' \Big/ \int_0^{t_{rest}} v(t')\, dt'. \tag{28}$$

We consider integrating over the first phase of the motion, during which the trajectory from (ψ_0, v_0) stays close to the stable manifold and approaches the saddle point which we denote by (v_{sp}, ψ_{sp}). Explicitly looking for an equilibrium point of (17) we find

$$v_{sp} = \exp[(\mu_* - \tan\alpha)/(b-a)], \quad \psi_{sp} := \psi_{ss}(v_{sp}) = 1/v_{sp}. \tag{29}$$

The critical case, in which the block covers the largest finite distance before stopping, is given by starting from an initial condition (v_0, ψ_0) on the stable manifold. For initial interfacial states that are rough, we have $\tanh(\psi_0/2) \approx 1$, so that the ψ_0-dependence can essentially be ignored. The (dimensional) persistence length, after which the block stops sliding can therefore be estimated to be

$$x_k = -\eta L \ln\left[\tanh(\psi_{sp}/2)\right] \quad \text{where} \quad \psi_{sp} = \exp[-(\mu_* - \tan\alpha)/(b-a)]. \tag{30}$$

In most cases, we can assume that $\psi_{sp} \ll 1$ and so approximate $\tanh\psi_{sp} \approx \psi_{sp}$ to obtain

$$x_k \approx \eta L\left(\ln 2 + \frac{\mu_* - \tan\alpha}{b-a}\right) = \eta L \frac{\mu_{ss}(V_*/2) - \tan\alpha}{b-a}. \tag{31}$$

Perhaps surprisingly, this expression indicates that x_k has a finite, and non-zero, limit as $\alpha \to 0$:

$$x_k^0 := \lim_{\alpha\to 0} x_k = \eta L\,[\ln 2 + \mu_*/(b-a)] = \eta L \frac{\mu_{ss}(V_*/2)}{b-a},$$

where $\mu_{ss}(\bar{v}) = \mu_* - (b-a)\ln(\bar{v}/V_*)$ refers to the steady-state friction coefficient, assuming that the interfacial state ψ has relaxed to its equilibrium value $\psi_{ss} = 1/v$. The existence of the limiting value x_k^0 suggests that we can use measurements of the persistence length, extrapolated to the limit $\alpha \to 0$, together with estimates of the slope of the curve $x_k(\alpha)$ for small α, as we expect this to be linear in $\tan\alpha$, in order to determine, jointly, the memory length L, the reference friction coefficient μ_*, and the reference velocity V_*.

It is clearly necessary that $\tan\alpha < \mu_{ss}(V_*/2)$ in order for the linear $\tan\alpha$-dependence of x_k, as implied by (31), to make sense. However, we note that approximation (31) provides a lower bound estimate for the *angle of friction* $\alpha_f \approx \tan^{-1}[\mu_{ss}(V_*/2)] = \tan^{-1}[\mu_* + (b-a)\ln(2)]$ from which the block becomes unable to stay still on the slope. For parameters of Table 2, we have $\alpha_f \approx 0.362$. Fig. 9 shows the numerically determined dependence of the persistence length (31) on the slope angle α.

Continuing our comparison with Rabinowicz's argument, we interpret (22) as the dimensionless critical block fracture energy $\mathcal{G}$ (Palmer and Rice, 1973; Ohnaka and Yamashita, 1989)

$$\mathcal{G} := (\mu_s - \tan\alpha)(x_k/L) = K(l_k/L)\tan\alpha, \tag{32}$$

that is required to set the block sliding unboundedly. Together with (31), (32) implies the relation

$$l_k \tan\alpha = \frac{\eta L(\mu_s - \tan\alpha)(\mu_{ss}(V_*/2) - \tan\alpha)}{K(b-a)}. \tag{33}$$

Experimental measurements of the critical release distance l_k over a range of slope angles α should therefore give a parabola when $l_k \tan\alpha$ is plotted as a function of $\tan\alpha$. This derivation of the functional form of the relation between $\tan\alpha$ and $l_k \tan\alpha$ allows straightforward determination of the effective static friction coefficient μ_s since it is clearly a zero of the curve.

Table 2
Material parameter values for the generalised spinodal friction law (2) and (10) used to fit the experimental data obtained for the frictional properties of Bristol paper board (Heslot et al., 1994).

μ_*	a	b	b/a	$b-a$	L (m)	V_* (ms^{-1})	c	$R = t_{**}V_*/L$
0.369	0.0349	0.0489	1.4011	0.014	0.9×10^{-6}	10^{-6}	10^{-3}	100

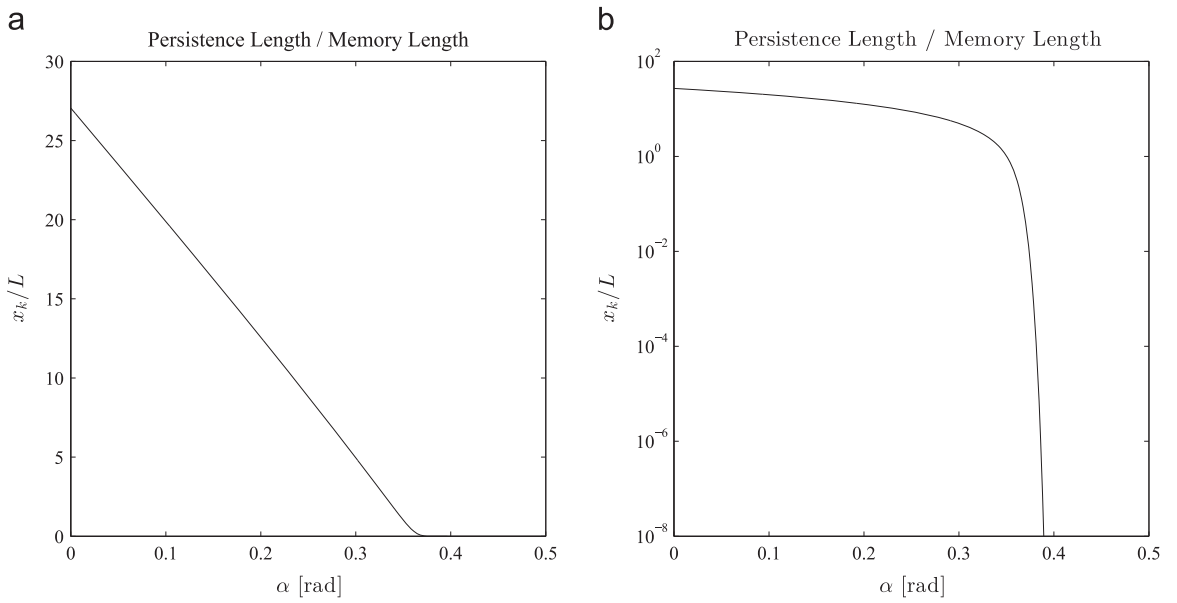

Fig. 9. Persistence length x_k as a function of slope angle α showing the linear dependence at small slope angles and rapid drop near the critical slope angle $\alpha \approx 0.38$. (a) Linear axes, to emphasise the behaviour at small α; (b) logarithmic plot to show the existence of the critical slope angle $\alpha \approx 0.38$.

4.3. Analytic estimates for the stable manifold

The position of the stable manifold of the saddle point (assuming that it exists) is a key part of all our discussions since it separates initial conditions into two sets: those that lead eventually to the block stopping (or at least, moving extremely slowly), and those that lead to unbounded (or at least extremely rapid) motion. In this section we present two approximate schemes for estimating the location of the stable manifold of the saddle point (v_{sp}, ψ_{sp}): this is an intrinsically highly nonlinear problem.

Standard methods for computing an approximate form for the stable manifold as a function, say $\psi = S(v)$, involve Taylor series expansions of the vector field close to the saddle point (v_{sp}, ψ_{sp}). We carried out this analytic computation but found that the resulting power series expansions (up to 14th order in $v - v_{sp}$!) were accurate only within a small neighbourhood of (v_{sp}, ψ_{sp}). In particular, the Taylor series argument fails accurately to capture the sharp 'knees' that the stable manifold contains, as illustrated, for example, in Fig. 7. This figure shows that the stable manifold is almost flat near the saddle point but becomes almost vertical further away, both above and below v_{sp}. The location of these vertical sections contains essential information concerning the size of velocity perturbations required to move trajectories from one set of initial conditions to the other.

A straightforward analytic estimate of these critical values of v can be obtained as follows. If we assume that the stable manifold is exactly horizontal near (v_{sp}, ψ_{sp}) and then vertical after passing through each sharp 'knee' then the location of the knees may be estimated by setting $\psi = \psi_{sp}$ and examining where $d(\ln \psi)/d(\ln v) = 1$, i.e. the gradient of the stable manifold (in log coordinates) passes through unity. This results in the condition

$$\chi(v) := \left.\frac{d(\ln \psi)}{d(\ln v)}\right|_{\psi=\psi_{sp}} = \frac{v}{\psi_{sp}} \frac{\epsilon^2 \sinh[\psi_{sp} - \psi_{ss}(v)]}{\eta \psi_{ss}(v)[\mu(v, \psi_{sp}) \cos\alpha - \sin\alpha]} = 1, \tag{34}$$

where $\psi_{sp} = \exp[-(\mu_* - \tan\alpha)/(b-a)]$, $\psi_{ss}(v) = 1/v$, and $\mu(v, \psi_{sp}) = \mu_* + a \ln v + b \ln \psi_{sp}$. This last expression follows from (9), setting $\psi = \tilde{\phi}$ and $c = 0$ since from Figs. 7(a) and 7(b) it is clear that the generalised Dieterich (ageing) law and the generalised spinodal law are almost identical near the saddle point and its stable manifold. Then we use the approximation $\sinh^{-1}(x) \approx \ln(2x)$ to simplify (9) to obtain $\mu(v, \psi)$ in the form given.

Fig.10 plots $\chi(v)$ as a function of v for four values of the slope angle α.

We observe that for this range of slope angles there are exactly two critical values $v_\pm$ (using the convention $v_- < v_{sp} < v_+$) at which $\chi(v_\pm) = 1$. v_- provides an upper bound on the location of the part of the stable manifold that lies in $\psi < \psi_{sp}$ while v_+ provides a lower bound on the location of the stable manifold in $\psi > \psi_{sp}$. For $\alpha = 0.34$ (the solid line in Fig. 10), the corresponding values are $v_- \approx 0.0503$ and $v_+ \approx 1312.6$. These are in reasonable agreement with the location of the lower-left and upper-right positions of the stable manifold, as shown in Fig. 7(a).

A refinement of this idea that gives more accurate results is as follows. First impose the change of variables $x = \ln(v/v_{sp})$ and $y = \ln(\psi/\psi_{sp})$, moving the saddle point to the origin $x = y = 0$, to obtain

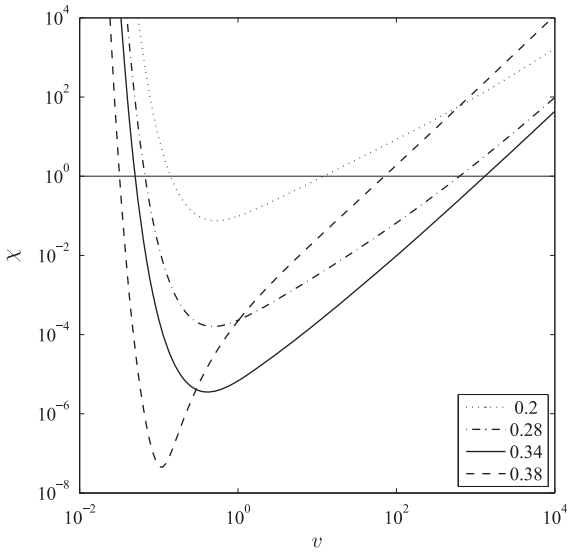

Fig. 10. Plot of $\chi(v)$, defined in (34), as a function of v for slope angles $\alpha \in \{0.2, 0.28, 0.34, 0.38\}$. Points where $\chi(v) = 1$ indicate the approximate location of the vertical sections of the stable manifold of (v_{sp}, ψ_{sp}) at small and large v.

$$\begin{cases} \dot{x} = -(Ax + By)e^{-x} =: f(x, y), \\ \dot{y} = e^{x-y}\sinh\{\psi_{sp}[e^{-x} - e^{y}]\}/\psi_{sp}^2 =: g(x, y), \end{cases} \tag{35}$$

where $A = a\cos(\alpha)/(\epsilon^2 v_{sp})$ and $B = b\cos(\alpha)/(\epsilon^2 v_{sp})$. The values in Table 2 imply that typically $A, B \sim O(10^5) \gg 1$. We compute the Jacobian matrix J at $x = y = 0$ and the corresponding matrix P of eigenvectors:

$$\mathrm{J} = \begin{pmatrix} -A & -B \\ -\psi_{sp}^{-1} & -\psi_{sp}^{-1} \end{pmatrix}, \quad \text{and} \quad \mathrm{P} = \begin{pmatrix} B & B \\ -A - \lambda_- & -A - \lambda_+ \end{pmatrix},$$

where $\lambda_- < 0 < \lambda_+$ are the eigenvalues $\lambda_\pm = (\mathrm{tr}\,\mathrm{J} \pm \sqrt{\Delta})/2$ of J whose discriminant $\Delta = (\mathrm{tr}\,\mathrm{J})^2 - 4\det\mathrm{J} > 0$.[5] The change of variables $(x, y)^{\mathrm{T}} = \mathrm{P}(X, Y)^{\mathrm{T}}$, i.e.

$$x = B(X + Y) \quad \text{and} \quad y = -(A + \lambda_-)X - (A + \lambda_+)Y, \tag{36}$$

leads to the system

$$\begin{cases} \dot{X} = \left[(A + \lambda_+)f(x, y) + Bg(x, y)\right]/\left(B\sqrt{\Delta}\right), \\ \dot{Y} = -\left[(A + \lambda_-)f(x, y) + Bg(x, y)\right]/\left(B\sqrt{\Delta}\right), \end{cases} \tag{37}$$

where $f(x, y)$ and $g(x, y)$, defined in (35), can be expressed as functions of (X,Y) through (36).

Fig. 11(a) (which is a linear–linear plot) indicates that in the (X,Y) coordinates, far from the origin, the stable manifold resembles lines of constant slope -1, i.e. $Y = S(X) \sim -X + C_\pm$ for some constants $C_\pm$. The constants $C_\pm$ relate to $v_\pm$ respectively, since the part of the stable manifold in $X > 0$ and $Y < 0$ corresponds to $v > v_{sp}$.

This suggests that $X = C_\pm$ can be estimated as the points where trajectories on the line $Y = 0$ in the (X,Y) plane achieve gradients close to -1, i.e. we solve the equation

$$\left.\frac{dY}{dX}\right|_{(C_\pm,0)} \equiv \left.\frac{\dot{Y}}{\dot{X}}\right|_{(C_\pm,0)} = -\xi, \tag{38}$$

where the coefficient ξ takes a fixed value close to unity. We find numerically that $\xi = 0.9$ gives a very good approximation, see Fig. 11(b). Working back through the changes of coordinates we see that the critical velocities $v_\pm$ are estimated by

$$v_\pm = v_{sp}\exp(BX_\pm). \tag{39}$$

Fig. 11(b) compares the numerical estimates for $v_\pm$ derived above (indicated by the solid lines) with the exact values deduced directly from computing the sable manifold (+ symbols). At small and large slope angles $v_\pm$ converge to v_{sp}: at intermediate

[5] Note that for the parameter values in Table 2 $\lambda_- \approx -A$ and $\lambda_+ \approx (b/a - 1)v_{sp}$.

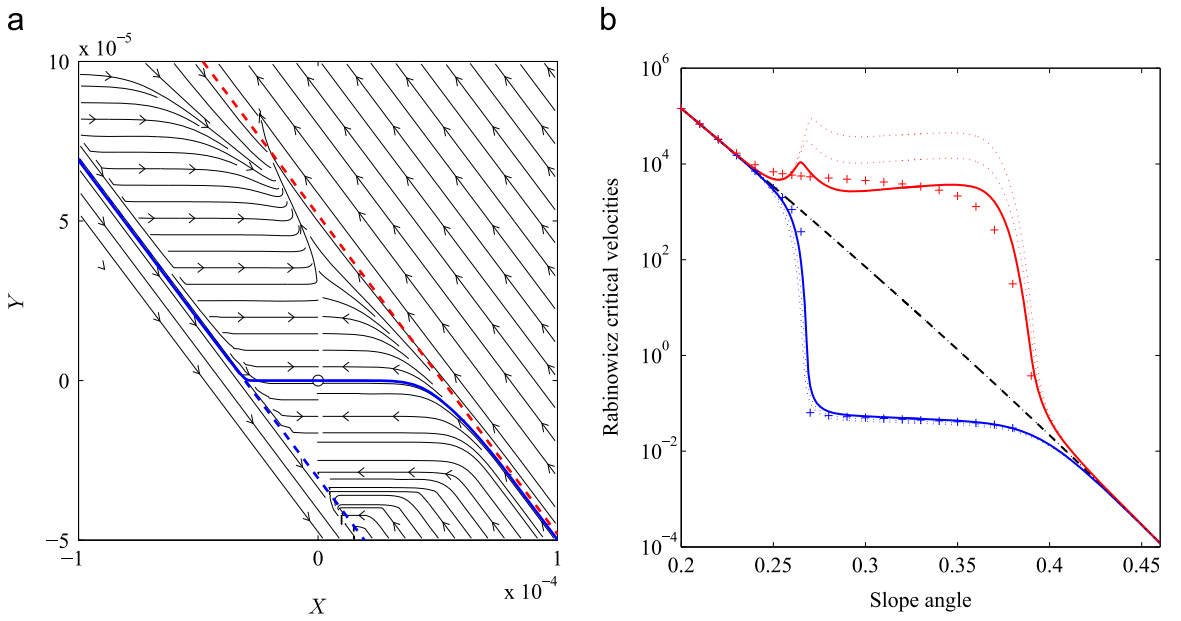

Fig. 11. Asymptotic approximation of the saddle point stable manifold, Rabinowicz's critical velocities and the corresponding estimation of the static friction coefficient. (a) Phase portrait of (37) and the generalised Dieterich law (5) within the phase space (X,Y), cf. Section 4.3 ($\alpha = 0.34$); (b) Rabinowicz's critical velocities as a function of α giving the location of the stable manifold of the saddle node at small (blue) and large (red) v. Numerical approximation from (38) and (39) for $\xi = \{0.9, 0.99, 0.999\}$ (thick solid lines correspond to $\xi = 0.9$). Symbols + represent the 'exact' critical velocities $v_{\pm}$ calculated from the direct numerical integration of the stable manifold equation. The dashed line designates the equilibrium slip rate of the saddle node $v_{sp}(\alpha)$. (For interpretation of the references to color in this figure caption, the reader is referred to the web version of this article.)

angles α, v_+ and v_- separate, indicating the quantitative dependence of the critical velocity for sustained slip on the initial smoothness of the interface.

We now use the value of the larger critical velocity v_+ to provide a theoretical estimate the value of the static friction coefficient that would be obtained in an experiment of the kind that Rabinowicz proposed, as summarised in Section 4.1. Assuming that the friction coefficient takes the constant value μ_s, combining the expression for the slip distance (26) with the energy conservation equation obtained by multiplying $(17)_1$ by v, and time-integrating from an initial state (v_0, ψ_0) to a final state (v, ψ) we obtain the energy balance equation

$$\epsilon^2(v^2 - v_0^2)/2 = \eta \cos\alpha(\mu_s - \tan\alpha) \ln\left[\tanh(\psi/2)/\tanh(\psi_0/2)\right]. \tag{40}$$

Starting from the critical velocity for a rough interface, i.e. setting $v_0 = v_+$ and taking $\psi_0 \gg 1$ we expect to end up at the saddle point, i.e. $(v, \psi) = (v_{sp}, \psi_{sp})$. Rearranging (27) in this case leads to an estimate for the static friction coefficient:

$$\mu_s \approx \tan\alpha + \epsilon^2(v_{sp}^2 - v_+^2)/\{2\eta \cos\alpha \ln[\tanh(\psi_{sp}/2)]\}. \tag{41}$$

Fig. 12(a) compares the estimates of μ_s calculated with (41) from the values of v_+ both computed approximately as explained above for different values of ξ ($\xi = 0.85$ allowing a good fit of the stable manifold) and numerically from the direct numerical integration of the non-autonomous differential equation $dS/dX = \dot{Y}/\dot{X}$ that the stable manifold equation $Y := S(X)$ must satisfy. We see that the numerical μ_s (red solid line) slightly fluctuates and linearly increases before diverging fast from a slope angle $\alpha \approx 0.39$. This effect is caused by the persistence length to vanish above a critical slope that can be evaluated from the asymptotic expansion $\tanh(x) \sim 1 - 2\exp(-2x)$ for large x. Used in the definition of the persistence length (30), we obtain

$$\alpha_f \equiv \tan^{-1}\left\{\mu_* + (b-a)\ln[\ln(2\eta/\varepsilon)]\right\}, \tag{42}$$

where ε measures how small we wish x_k/L to be. For $\varepsilon \sim 10^{-16}$ about machine precision, $\alpha_f \approx 0.397$. In addition to this, we emphasise that the dimensionless critical fracture energy $\mathcal{G}$ (32) also drops to zero as α approaches α_f as shown in Fig. 11(d).

To conclude, we propose to identify α_f as the block *friction angle* (or angle of repose) from which the block starts sliding as is observed in the variable slope angle high school block experiment. Such phenomenon is then physically explained by the evanescence of the persistence length at $\alpha = \alpha_f$. In this interpretation, the static friction coefficient (28) becomes undefined at the friction angle. Nevertheless, following the empirical definition of the static coefficient would lead to

$$\mu_s^f := \tan^{-1}(\alpha_f) \approx 0.378, \tag{43}$$

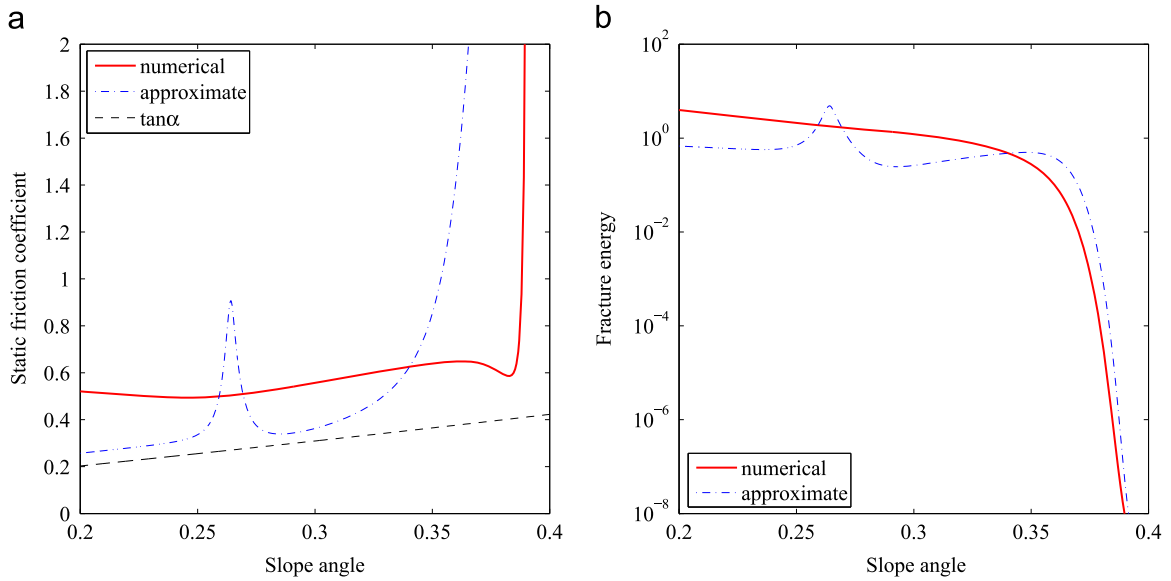

Fig. 12. Effect of slope angle α on: (a) the static friction coefficient μ_s estimates given (41) for both the numerical and approximate computations of v_+, and (b) the block 'fracture energy' defined by $\mathcal{G}$ (32). Notice the divergence of μ_s and the rapid drop of $\mathcal{G}$ caused by annihilation of the persistence length as α tends to the friction angle α_f (42).

which is noticeably lower from the estimation of μ_s from (28) for sub-critical slope angle $\alpha < \alpha_f$. The use of static friction coefficient might then be misleading, predicting a smaller frictional resistance.

Alternatively, the values of μ_s that we calculate from the stable manifold asymptotic location, in particular the divergence of μ_s as $\alpha \to \alpha_f$, may explain both the observed dispersion within stiction experimental measurements and the high values of the static friction coefficient experimentally measured (e.g. Rabinowicz, 1951; Byerlee, 1978), provided the corresponding measurements result from initial energy inputs à la Rabinowicz. Applying the method to (41), we find numerically that $\mu_s \approx 0.621$, $v_+ \approx 10^{3.45} \approx 2.81 \times 10^3$, $x_k/L \approx 1.775$ and $\mathcal{G} \approx 0.475$ for $\alpha = 0.34$ and $\xi = 0.85$.

4.4. Phases of sliding behaviour

The overall behaviour of solutions to (17) is summarised in Fig. 13 which shows phase portraits for the generalised Dieterich law and the spinodal law. In the preceding Sections 4.2 and 4.3 we discussed the initial phase of the motion starting from a high velocity, rough interface state. After the initial phase, for both friction laws, we see that trajectories evolve in a second phase to lie very close to the $\dot{v} = 0$ nullcline, shown by the dashed lines in Fig. 13. In this phase, when neither v nor ψ is particularly small, the constraint on the dynamics is provided by the small value of the parameter ϵ which ensures that the motion evolves subject to $\dot{v} = 0$. For the parameters in Table 2, $\epsilon \sim 10^{-4}$. This phase describes the slowing and roughening of the interface at longer times.

What is perhaps more surprising is that, as ψ increases and v decreases further, there is a transition to another, third, phase. The third phase arises when v decreases below the critical velocity v_-. In this third phase the trajectory leaves the vicinity of the nullcline $\dot{v} = 0$ and moves across towards the nullcline $\dot{\psi} = 0$. Although this is a low-speed part of the dynamics, this behaviour is observed only when the full form of the state equation $(4)_2$ is used, and not the linearised version. The key to this observation is that at low velocities the relevant values of ψ are large, and so the nonlinear form of the $\sinh[\psi - \psi_{ss}(v)]$ function becomes important.

For the generalised Dieterich law, Fig. 13(a), this third phase continues indefinitely: trajectories remain close to the $\dot{\psi} = 0$-nullcline and the interface continues to slow down, and roughens without bound, at long times.

Fig. 14 illustrates the dynamics within each of these three phases. Fig. 14(a) plots μ, v and ψ as functions of distance x. Fig. 14(b) shows the evolution of v and ψ as functions of time t. Fig. 14(c) shows the friction coefficient μ and the position of the block x as functions of t. In the first phase, the three plots in Fig. 14(a) show that μ, v and ψ all decrease, over $0 \le x < 0.325$ approximately.

In the second phase, approximately the region $0.325 < x < 0.494$, μ is constant (as must be the case, since $(17)_1$ shows that μ is very close to $\tan\alpha$ when $\dot{v} = 0$), while v decreases and $\psi \sim 1/v$ increases. In the third phase, $x > 0.494$, μ and ψ increase rapidly while v becomes extremely small, so the block effectively stops moving.

Turning now to the spinodal law, Fig. 13(b) shows, as we expect, that the first two phases of the motion closely resemble the Dieterich case. The third phase differs since the existence of the stable equilibrium point at small v and large ψ means that trajectories stay closer to the v-nullcline and are ultimately attracted to the equilibrium, so that ψ remains bounded at long times. Since ψ remains bounded, the friction coefficient μ also remains bounded: compare the upper plots in Figs. 15(a) and (c) with those

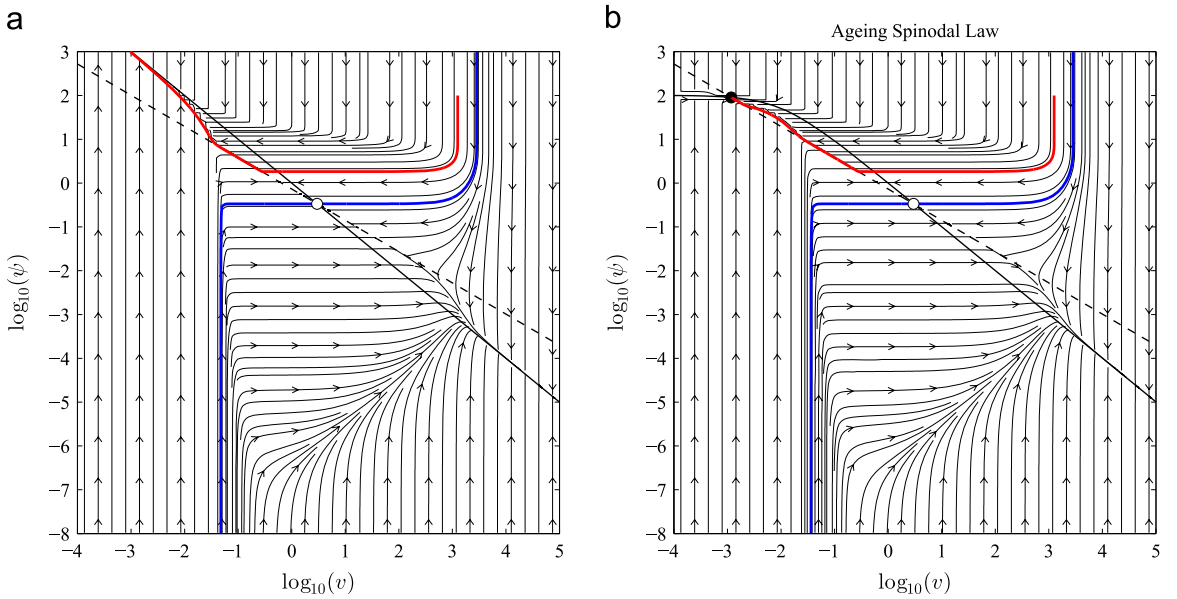

Fig. 13. Phase portraits for (a) the generalised Dieterich law; and (b) the spinodal law. The spinodal law has a stable equilibrium point at low velocity (due to the existence of a local maximum in $\mu_{ss}(v)$) in addition to the saddle point whose stable manifold, in both plots, is shown as the solid blue line. The other solid (red) line is the trajectory starting from the rough, high velocity initial condition $(v_0, \psi_0) = (10^{3.1}, 100)$ above the stable manifold. Slope angle $\alpha = 0.34$. Dashed and solid lines indicate the v-nullcline $\mu(v, \psi) = \tan\alpha$ and ψ-nullcline $\psi = \psi_{ss}(v)$, respectively. (For interpretation of the references to color in this figure caption, the reader is referred to the web version of this article.)

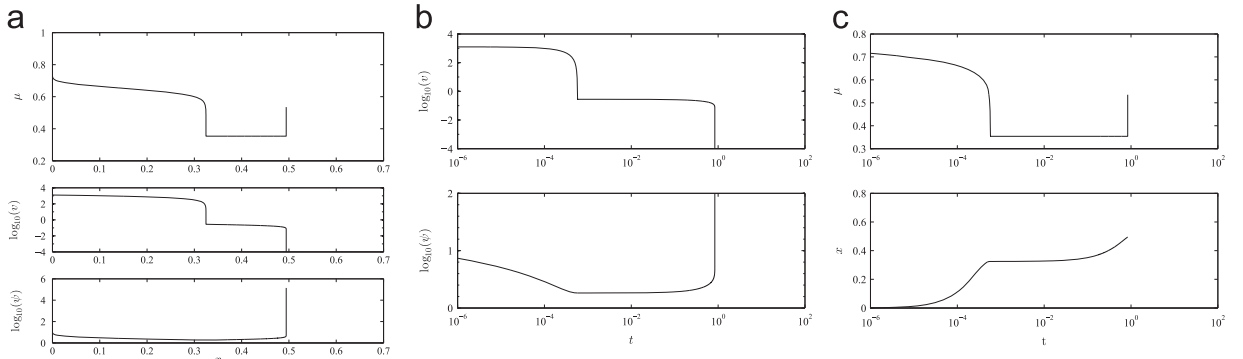

Fig. 14. Slip dynamics for the generalised Dieterich law. Initial condition $(v_0, \psi_0) = (10^{3.1}, 100)$, slope angle $\alpha = 0.34$.

in Figs. 14(a) and (c). This boundedness of μ is important on physical grounds since, although the interface roughens over time, this healing process in (quasi-)stationary contact should not continue indefinitely.

In terms of interpreting Rabinowicz's experimental results, however, the difference between use of the generalised Dieterich or spinodal laws is not likely to be significant. Nevertheless, the use of the full nonlinear kinetics given by $(4)_2$ is important since using the full kinetics changes the vector field significantly in two regions of the (v, ϕ) phase plane: when both v and ϕ are very large, and when both v and ϕ are very small, i.e. the top right and bottom left corners of the phase plane plots. In both regions the trajectories for the full nonlinear kinetics (the 'generalised' versions of the friction laws), shown in Fig. 7, are much closer to vertical than in the case of the linearised 'first order kinetics' version illustrated in Fig. 6. This is because in both these regions we are far from the nullcline $\psi = 0$, i.e. we have $|\psi - \psi_{ss}(v)| \gg 1$ and hence the form trajectories take is influenced substantially by the nonlinearity of the sinh function.

5. Conclusions

In this paper we provide detailed analysis that links rate-and-state friction with Coulomb's proposition of two distinct, constant, coefficients describing static and dynamic friction forces, and denoted μ_s and μ_k, respectively.

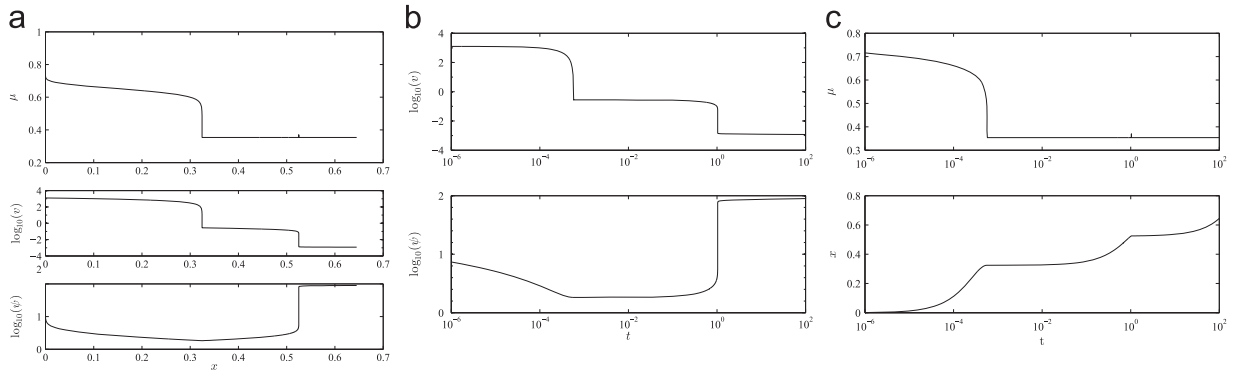

Fig. 15. Slip dynamics for the spinodal law. Initial condition $(v_0, \psi_0) = (10^{3.1}, 100)$, slope angle $\alpha = 0.34$.

We firstly review a number of different formulations for rate-and-state friction and we show in Section 2 that they can be put into a common framework given by (4). This illustrates their strong similarities, clarifies the points of difference between them, and allows the development of further rate-and-state formulations. One of these extensions, the spinodal law (9)–(10), remedies some unphysical features of the Dieterich/Ruina expressions. We have discussed this is in detail previously elsewhere (Putelat et al., 2007, 2008, 2010, 2011).

In essence, friction laws derived from the framework (4) are phenomenologically distinguished through the choices of the functions ψ, $\theta(\psi)$, $\psi_{ss}(v)$ and $t_\star(v)$. We expect these functions in general to depend also on normal stress, temperature and wear parameters. This framework enables us to capture the historical dichotomy between the Dieterich (ageing) and Ruina (slip) laws, by stating their generalisations as follows. For the choices $\theta(\psi) := \ln(\psi)$ and $t_\star(v) := t_{**}\psi_{ss}(v)$, we define the generalised ageing law

$$\begin{cases} \mu = a\,\sinh^{-1}\left\{(v/2)\exp\left[(\mu_* + b\ln(\psi))/a\right]\right\}, \\ \dot{\psi} = -\ \sinh(\psi - \psi_{ss}(v))/(t_{**}\psi_{ss}(v)), \end{cases} \tag{44}$$

while the choices $\theta(\psi) := \psi$ and $t_\star(v) := t_{**}\exp(\psi_{ss})$, enable us to define the generalised slip law

$$\begin{cases} \mu = a\,\sinh^{-1}\left\{(v/2)\exp\left[(\mu_* + b\,\psi)/a\right]\right\}, \\ \dot{\psi} = -\ \sinh\left(\psi - \psi_{ss}(v)\right)/\left(t_{**}\exp(\psi_{ss}(v))\right). \end{cases} \tag{45}$$

In both cases this description requires a statement of the equilibrium state $\psi_{ss}(v)$ in order to be complete: the determination of $\psi_{ss}(v)$ can be made using experimental data, as we described in previous work (Putelat et al., 2010, 2011).

We note also that in Putelat et al., 2011 we considered a commonly used alternative expression to $(4)_1$ based on the "Bowden–Tabor product decomposition" of the interfacial shear stress motivated by some interfacial asperity deformation, i.e.

$$\tilde{\tau} \equiv \tilde{A}_r(\psi)\tilde{\tau}_c(\tilde{v}), \tag{46}$$

where $\tilde{A}_r$ is the real interfacial contact area and $\tilde{\tau}_c$ is a measure of asperity yield or creep stress whose slip rate dependence is also justified by some thermally activated rate process. Within this alternative framework, depending on the asperity deformation mechanism that is assumed, we also showed that the state dependence of the real contact area A_r can introduce non-monotonic variations for the steady-state friction coefficient $\mu_{ss}(\tilde{v}) := \mu[\tilde{v}, \psi_{ss}(\tilde{v})]$. However there are dynamical differences, for example in Putelat et al. (2010) we reported that for a driven spring-block system such friction models, based on (46), predict a subcritical instability of steady sliding (a Hopf bifurcation leading to stick-slip dynamics) at low driving velocity which is in disagreement with the experimental characterisation of the stick-slip boundary described as a supercritical Hopf bifurcation in Baumberger et al. (1994) and Heslot et al. (1994).

In additional work, not reported here, we have compared the phase portraits presented above with those obtained using two friction coefficients that are motivated by the Bowden–Tabor product decomposition and discussed in detail in section 5 of Putelat et al. (2010). These friction coefficients are minor modifications of those proposed by Heslot et al. (1994), Baumberger et al. (1999), Berthoud et al. (1999), Persson (2000) and Brechet and Estrin (1994), Estrin and Brechet (1996). We find that the geometrical features of the phase portrait for the sliding block are qualitatively similar to those presented above using (4). We conclude that the key similarity is the non-monotonicity of the steady state friction curve $\mu_{ss}(\tilde{v})$, and hence in the present paper we chose to focus the discussion on the framework given by (4).

The first context in which we link Coulomb friction with the rate-and-state formalism is in considering the stability of the steady-state motion of a block sliding on an inclined plane, in Section 3. When the interface is sliding at constant velocity we interpret the static friction coefficient as the local maximum of the steady-state friction coefficient, present at

small slip rates. Comparison between predictions from the classical monotonic rate-and-state laws suggests that non-monotonic laws with a section over which friction strengthens with increasing velocity, at low velocities, are better physical models for sliding. Monotonic steady-state friction laws do not allow the saddle point equilibrium (corresponding to unstable steady sliding) to disappear for small slope angles; monotonic friction laws therefore always allow high-velocity sliding to develop, unphysically, if the interface is initially very smooth. For spinodal rate-and-state friction laws, we demonstrate the existence of a region of bistability (two stable equilibria representing steady sliding at different velocities) that opens up as the parameter c describing the residual strength of the interface at high velocities increases, as shown in Fig. 4.

In Section 4 we turn to a different dynamical setting in which a stationary block of material placed on a slope of constant angle α to the horizontal is impulsively set into motion by an impact. This section is motivated by the experimental results and theoretical arguments put forward by Rabinowicz (1951) concerning the 'persistence length' over which the coefficient of friction could be said to remain at its static value μ_s before dropping to the kinetic value μ_k. This idea of a distance s_k that is a 'limit of the persistence of the static coefficient of friction' (Rabinowicz, 1951, p. 1374) is an attempt to extend Coulomb's idea of friction. Clearly, the rate-and-state formalism is also an attempt to extend Coulomb friction but it is much more closely based on physical intuition. Our results show that the idea of a persistence length s_k can be related quantitatively to the rate-and-state formalism. Moreover, s_k, and indeed the value of the static friction coefficient μ_s, can be estimated analytically from parameters in the rate-and-state description by realising that s_k corresponds to the block slip distance along the stable manifold of the system saddle equilibrium point which exists for moderate slope angles. We deduce an expression (28) that yields μ_s as a velocity-weighted average of the rate-and-state friction coefficient over the motion of the block. Analytic estimates of the stable manifold which follow energy conservation then furnish us with an approximate approach (41) that estimates effectively the value of μ_s, defined by (28). Similarly, denoting the persistence length that would be deduced from the rate-and-state formalism by x_k, we derive the relation (30) that expresses x_k in terms of parameters in the rate-and-state model, in particular the memory length L, see Fig. 9. We conclude that it does make sense to view the persistence length s_k as the macroscopic manisfestation of the microscopic memory length L.

Finally, in Section 4.4 we describe in detail the qualitative motion that the rate-and-state formalism produces, and we comment on the relation between the phases of the motion and the features of the rate-and-state model used. The evolution of sliding under rate-and-state friction is of course governed by the detailed geometry of the phase space which results from the specific model. From a dynamical systems perspective, the phase space is divided into two regimes (block arrest and block acceleration) by the stable manifold of the saddle point. We show that the shape of this stable manifold and the qualitative features of the vector field control the transient response of the interface to a sudden impulse, see Fig. 13. In particular, numerical time integration of the rate-and-state block equations of motion gives rise to the slip-controlled drop of the instantaneous friction coefficient as depicted by Rabinowicz, see Figs. 14 and 15. Rate-and-state friction also sheds light on the fact that Rabinowicz's persistence length corresponds to the upper bound of the actual macroscopic slip distance required for the block arrest and whose determination is set by the system initial conditions. We emphasise that the two key tribological features responsible for the regimes of block arrest and sustained sliding are the existence within the state evolution law of the nonlinear sinh-type kinetics, and the velocity-dependent dynamic interfacial rejuvenation.

In geophysical terms, our results have several implications. The main consequence of the existence of a bistable region in the spinodal friction law concerns landslide and slope stability. This bistability introduces a sensitivity to finite amplitude perturbations below the classical critical Coulomb angle $\alpha_c = \tan^{-1}(\mu_s)$. The critical angle α_{cm} which we introduce, and which is associated with the high-velocity sliding branch, would appear to be a better safety criterion than the safety factor estimated from the limit equilibrium analysis (Chowdhury et al., 2009). Our bistable model is in contrast to previous such models (e.g. Henley, 1976; Qin et al., 2001) due to its pure tribological origin; it has also the advantage of relying on only a single friction law. We note that the monotonic Ruina rate-and-state model has been used in the past for studying slope stability (Chau, 1995, 1999; Helmstetter et al., 2004). Regarding the mechanics of faults and thrusts, we suspect them to be more sensitive to finite amplitude perturbations as we expect the residual strength to reduce with increasing the normal stress, the bistability domain widening as a result, and the local minimum of friction being displaced towards larger slip rates as reported in Kilgore et al. (1993). We note also that the hysteretic behaviour favoured by spinodal friction may also explain the pulses of avalanches observed in gravity current of granular matter (Takagi et al., 2011). Another appealing application of spinodal friction is to model basal sliding involved in the flow of glaciers and ice sheets, see Fowler (1987), Fowler (1989), Sayag and Tziperman (2009), Sayag and Tziperman (2009). Note that rate-and-state friction has recently been proposed for taking into account experimental sliding memory effects reported for sea ice (Lishman et al., 2011, 2013).

Turning to earthquake mechanics, we suppose that the initial earthquake nucleation phase could be considered as an initial sudden input of kinetic energy comparable to the impact of the rolling ball on the block in Rabinowicz's experiments. Then the concept of persistence length (30) could be viewed as a slip nucleation length, assuming that the rate-and-state description of a geophysical fault is qualitatively similar to that for a sliding block. Of course, the equation of motion of the block $(17)_1$ is much simpler than the full equations for the elastodynamics of a fault. Nevertheless, we believe that the formula (30) derived for the persistence length may provide relevant physical insight into fault dynamics. This is because essentially (30) comes from integrating the state evolution law by itself, and this is valid during the fast initial phase of interfacial smoothing. As the persistence length x_k may be several orders of magnitude larger than the memory length L, we finally remark that expression (30) may explain why estimates of the nucleation length of fault from field data are much larger than the nucleation lengths observed at the scales of laboratory experiments (Scholz, 1998).

Acknowledgments

TP acknowledges support from the École Polytechnique and the UK EPSRC (grant ref. EP/K003836/1). JHPD is supported by a University Research Fellowship from the Royal Society. We also wish in particular to thank John Willis for his supportive comments and for many fruitful discussions, Herbert Huppert, and the ITG, DAMTP, University of Cambridge where parts of this work were carried out.

References

Archard, J.F., 1959. The temperature of rubbing surfaces. Wear 2, 438–455.
Bar-Sinai, Y., Spatschek, R., Brener, E.A., Bouchbinder, E., 2014. On the velocity-strengthening behavior of dry friction. J. Geophys. Res. 119, 1738–1748.
Baumberger, T., Berthoud, P., Caroli, C., 1999. Physical analysis of the state- and rate-dependent friction law: dynamic friction. Phys. Rev. B 60 (6), 3928–3939.
Baumberger, T., Caroli, C., 2006. Solid friction from stick-slip down to pinning and aging. Adv. Phys. 55 (3–4), 279–348.
Baumberger, T., Heslot, F., Perrin, B., 1994. Crossover from creep to inertial motion in friction dynamics. Nature 367, 544–546.
Beerler, N.M., Tullis, T.E., Weeks, J.D., 1994. The roles of time and displacement in the evolution effect in rock friction. Geophys. Res. Let. 21 (18), 1987–1990.
Berthoud, P., Baumberger, T., G'Sell, S., Hiver, J.-M., 1999. Physical analysis of the state- and rate-dependent friction law: static friction. Phys. Rev. B 59 (22), 14313–14327.
Bowden, F.P., Tabor, D., 1954. The Friction and Lubrication of Solids. Oxford—Clarendon Press.
Bréchet, Y., Estrin, Y., 1994. The effect of strain rate sensitivity on dynamic friction of metals. Scripta Met. Mater. 30, 1449–1454.
Byerlee, J.D., 1978. Friction of rocks. Pageoph 116, 615–626.
Chau, K.T., 1995. Landslides modeled as bifurcations of creeping slopes with nonlinear friction law. Int. J. Solids Struct. 32, 3451–3464.
Chau, K.T., 1999. Onset of natural terrain landslides modelled by linear stability analysis of creeping slopes with a two-state variable friction law. Int. J. Numer. Anal. Meth. Geomech. 23, 1835–1855.
Chowdhury, R., Flentje, P., Bhattacharya, G., 2009. Geotechnical Slope Analysis. CRC Press, The Netherlands.
di Bernardo, M., Champneys, A.R., Budd, C.J., Kowalczyk, P., 2008. Piecewise-smooth Dynamical Systems, Applied Mathematical Sciences, vol. 163. Springer, London.
Dieterich, J.H., 1978. Time-dependent friction and the mechanics of stick-slip. Pageoph 116, 790–806.
Dieterich, J.H., 1979. Modeling rock friction: 1. experimental results and constitutive equations. J. Geophys. Res. 84, 2161–2168.
Doedel, E.J., Keller, H.B., Kernevez, J.P., 1991. Numerical analysis and control of bifurcation problems. Int. J. Bifurc. Chaos 1 (3), 493–520. AUTO 2000 available via Internet from ⟨http://indy.cs.concordia.ca/auto/⟩.
Duvaut, G., Lions, J.L., 1976. Inequalities in Mechanics and Physics. Grundlehren der mathematischen Wissenschaften. Springer-Verlag, Berlin, Heidelberg, New York.
Estrin, Y., Bréchet, Y., 1996. On a model of frictional sliding. Pure Appl. Geophys. 147 (4), 745–762.
Fowler, A.C., 1987. A theory of glacier surges. J. Geophys. Res.: Solid Earth 92 (B9), 9111–9120.
Fowler, A.C., 1989. A mathematical analysis of glacier surges. SIAM J. Appl. Math. 49, 246–262.
Grosch, K.A., 1963. The relation between the frictional and visco-elastic properties of rubber. Proc. R. Soc. Lond. A 274, 21–39.
Gu, J.C., Rice, J.R., Ruina, A.L., Tse, S.T., 1984. Slip motion and stability of a single degree of freedom elastic system with rate and state dependent friction. J. Mech. Phys. Solids 32, 167–196.
Helmstetter, A., Sornette, D., Grasso, J.-R., Andersen, J.V., Gluzman, S., Pisarenko, V., 2004. Slider block friction model for landslides: application to Vaiont and La Clapière landslides. J. Geophys. Res.: Solid Earth 109 (B2).
Henley, S., 1976. Catastrophe theory models in geology. J. Int. Assoc. Math. Geol. 8, 649–655.
Heslot, F., Baumberger, T., Perrin, B., Caroli, B., Caroli, C., 1994. Creep, stick-slip, and dry-friction dynamics: experiments and a heuristic model. Phys. Rev. E 49, 4973–4988.
Hulikal, S., Bhattacharya, K., Lapusta, N., 2015. Collective behavior of viscoelastic asperities as a model for static and kinetic friction. J. Mech. Phys. Solids 76, 144–161, http://dx.doi.org/10.1016/j.jmps.2014.10.008.
Kato, N., Tullis, T.E., 2001. A composite rate- and state-dependent law for rock friction. Geophys. Res. Lett. 28 (6), 1103–1106.
Kato, N., Tullis, T.E., 2003. Numerical simulation of seismic cycles with a composite rate- and state-dependent friction law. Bull. Seismol. Soc. Am. 93 (6), 841–853.
Kilgore, B.D., Blanpied, M.L., Dieterich, J.H., 1993. Velocity dependent friction of granite over a wide range of conditions. Geophys. Res. Lett. 20 (10), 903–906.
Lishman, B., Sammonds, P.R., Feltham, D.L., 2011. A rate and state friction law for saline ice. J. Geophys. Res.: Oceans 116 (C5). n/a–n/a.
Lishman, B., Sammonds, P.R., Feltham, D.L., 2013. Critical slip and time dependence in sea ice friction. Cold Reg. Sci. Technol. 91:9–13.
Marone, C., 1998. Laboratory-derived friction laws and their application to seismic faulting. Annu. Rev. Earth Sci. 26, 643–696.
Ohnaka, M., Yamashita, T., 1989. A cohesive zone model for dynamic shear faulting based on experimentally inferred constitutive relation and strong motion source parameters. J. Geophys. Res. 94, 4089–4104.
Palmer, A.C., Rice, J.R., 1973. The growth of slip surfaces in the progressive failure of overconsolidated clay. Proc. R. Soc. Lond. 332 (527–548).
Perrin, G., Rice, J.R., Zheng, G., 1995. Self-healing slip pulse on a frictional surface. J. Mech. Phys. Solids 43 (9), 1461–1495.
Persson, B.N.J., 2000. Sliding Friction: Physical Principles and Applications. Nanoscience and Technology, 2nd edition. Springer-Verlag, Berlin, Heidelberg, New York.
Persson, B.N.J., Albohr, O., Mancosuc, F., Peveric, V., Samoilov, V.N., Sivebaek, I.M., 2003. On the nature of the static friction, kinetic friction and creep. Wear 254, 835–851.
Putelat, T., Dawes, J.H.P., Willis, J.R., 2007. Sliding modes of two interacting frictional interfaces. J. Mech. Phys. Solids 55 (10), 2073–2105.
Putelat, T., Dawes, J.H.P., Willis, J.R., 2010. Regimes of frictional sliding of a spring-block system. J. Mech. Phys. Solids 58 (1), 27–53.
Putelat, T., Dawes, J.H.P., Willis, J.R., 2011. On the microphysical foundations of rate-and-state friction. J. Mech. Phys. Solids 59 (5), 1062–1075.
Putelat, T., Willis, J.R., Dawes, J.H.P., 2008. On the seismic cycle seen as a relaxation oscillation. Philos. Mag. 88, 3219–3243.
Qin, S., Jiao, J.J., Wang, S., Long, H., 2001. A nonlinear catastrophe model of instability of planar-slip slope and chaotic dynamical mechanisms of its evolutionary process. Int. J. Solids Struct. 38 (44–45), 8093–8109.
Rabinowicz, E., 1951. The nature of the static and kinetic coefficients of friction. J. Appl. Phys. 22 (11), 1373–1379.
Rabinowicz, E., 1957. The intrinsic variables affecting the stick-slip process. Proc. Phys. Soc. (Lond.) 71, 668–675.
Rabinowicz, E., 1995. Friction and Wear of Materials, 2nd edition. John Wiley & Sons, New York.
Rice, J.R., Ben-Zion, Y., 1996. Slip complexity in earthquake fault models. Proc. Natl Acad. Sci. USA 93, 3811–3818.
Rice, J.R., Lapusta, N., Ranjith, K., 2001. Rate and state dependent friction and the stability of sliding between elastically deformable solids. J. Mech. Phys. Solids 49, 1865–2198.
Rice, J.R., Ruina, A.L., 1983. Stability of steady frictional slipping. J. Appl. Mech. 50, 343–349.

Ruina, A.L., 1980. Friction Laws and Instabilities: a Quasistatic Analysis of Some Dry Frictional Behavior (Ph.D. thesis), Brown University.
Ruina, A.L., 1983. Slip instability and state variable friction laws. J. Geophys. Res. 88:10, 359-10, 370, 1983.
Sayag, R., Tziperman, E., 2009. Interaction and variability of ice streams under a triple-valued sliding law and non-newtonian rheology. J. Geophys. Res. 116, F01009.
Sayag, R., Tziperman, E., 2009. Spatiotemporal dynamics of ice streams due to a multivalued sliding law. J. Fluid Mech. 640, 483–505.
Scholz, C.H., 1998. Earthquakes and friction laws. Nature 391, 37–41.
Scholz, C.H., 2002. The Mechanics of Earthquakes and Faulting, 2nd edition. Cambridge University Press, Cambridge.
Shimamoto, T., 1986. Transition between frictional slip and ductile flow for halite shear zones at room temperature. Science 231, 711–714.
Takagi, D., McElwaine, J.N., Huppert, H.E., 2011. Shallow granular flows. Phys. Rev. E 83, 031306.
Tsutsumi, A., Shimamoto, T., 1997. High-velocity frictional properties of Gabbro. Geophys. Res. Lett. 24, 699–702.
Weeks, J.D., 1993. Constitutive laws for high-velocity frictional sliding and their influence on stress drop during unstable slip. J. Geophys. Res.: Solid Earth 98 (B10), 17637–17648.